

# Topology optimization of fluidic flows on 2-manifolds

Yongbo Deng<sup>1,2\*</sup>, Jan G. Korvink<sup>1†</sup>

<sup>1</sup> Institute of Microstructure Technology (IMT),  
Karlsruhe Institute of Technology (KIT),

Hermann-von-Helmholtzplatz 1, Eggenstein-Leopoldshafen 76344, Germany;

<sup>2</sup> State Key Laboratory of Applied Optics (SKLAO),  
Changchun Institute of Optics, Fine Mechanics and Physics (CIOMP),  
Chinese Academy of Sciences (CAS), Changchun 130033, China.

November 29, 2023

## Abstract

This paper presents a topology optimization approach for the fluidic flows on 2-manifolds or two-dimensional manifolds, which can represent the viscous and incompressible material surfaces. The fluidic motion on such a material surface can be described by the surface Navier-Stokes equations, which are derived by using the elementary tangential calculus in terms of exterior differential operators expressed in a Cartesian coordinate system. Based on the topology optimization model for fluidic flows with porous medium filling the design domain, an artificial Darcy friction is added to the area force term of the surface Navier-Stokes equations and the physical area forces are penalized to eliminate their existence in the fluidic regions and to avoid the invalidity of the porous medium model. Topology optimization for steady and unsteady surface flows can be implemented by iteratively evolving the impermeability of the porous medium on 2-manifolds, where the impermeability is interpolated by the material density derived from the design variable. The related partial differential equations are solved by using the surface finite element method. Numerical examples have been provided to demonstrate this topology optimization approach for fluidic flows on 2-manifolds.

**Keywords:** Topology optimization; 2-manifold; Fluidic flow; Material distribution method; Porous medium.

## 1 Introduction

Fluidic flows at material interfaces play key roles in flexible and wearable microfluidics [1]. The drawbacks, e.g., relatively expensive to process, brittle and not self-sealing, associated with silicon and glass led to the emergence of materials with the ability to deform, bend and stretch under mechanical loads, for developing the flexible microfluidics [2, 3]. Because of the mechanical and adhesion properties of soft and stretchable materials, the high sensitivity of efficient measurements at the micrometer size, great functional versatility on the integration with electronic modules, and the merits on low-cost and massive fabrication, microfluidics has become the excellent candidate of wearable devices [4]. The design space of fluidic structures was thus extended onto material interfaces in flexible and wearable microfluidics. To implement the robust and efficient inverse design of structures for fluidic flows on the extended design space, this paper presents a topology optimization approach for fluidic flows at material interfaces, which can be represented by the geometrical concept of 2-manifolds.

Optimization of structural topology was investigated as early as 1904 for trusses by Michell [5]. Material distribution method for topology optimization was pioneered by Bendsoe and Kikuchi for elasticity [6], and this method has been extended to a variety of areas, e.g., acoustics, electromagnetics, fluid dynamics and thermodynamics [7–20]. Several other methods also have been proposed and developed for the implementation of topology optimization, e.g., the level set method [21, 22], the evolutionary techniques [23–25], the evolutionary structural optimization method [26, 27], the method of moving morphable components [28, 29] and the phase field method [30]. In this paper, material distribution method is used to implement the topology optimization of fluidic flows on 2-manifolds.

---

\*yongbo.deng@kit.edu; dengyb@ciomp.ac.cn

†jan.korvink@kit.edu

Fluidic flows at material interfaces, i.e., fluidic flows on 2-manifolds, are important aspects of fluid mechanics. With regard to fluid mechanics, topology optimization has been implemented for Stokes flows [19], steady Navier-Stokes flows [20], creeping fluid flows [31], unsteady Navier-Stokes flows [32, 33], flows with body forces [34, 35], turbulent flows [36, 37], two-phase flows of immiscible fluids [38], electroosmotic flows [39, 40] and flows of non-Newtonian fluids [41, 42], etc. Topology optimization of fluidic flows have been reviewed in [43]. With regard to material interfaces, related investigations have been implemented for stiffness and multi-material structures [44–50], layouts of shell structures [51–56], electrode patterns of electroosmosis [40], fluid-structure and fluid-particle interaction [57–59], energy absorption [60], cohesion [61], actuation [62] and wettability control [63–65], etc.; a topology optimization approach implemented on 2-manifolds has also been generally developed with applications in the areas of wettability control, heat transfer and electromagnetics [66].

Fluidic flows at material interfaces for the interfacial phenomena, e.g., emulsions, foams and biological membranes, can be described by the surface Navier-Stokes equations defined on 2-manifolds for Newtonian surface fluids [67–72]. This can be dated back to Scriven who was interested in the importance of interface rheology on foam stability [67]. In topology optimization of flows problems, a porous medium model was developed for Stokes flows [19]. This model has been extended to implement topology optimization of steady Navier-Stokes flows [20] and unsteady Navier-Stokes flows [32, 33]. In this model, the porous medium was filled in the two-/three-dimensional design domains by introducing an artificial Darcy friction into the Stokes equations and Navier-Stokes equations. The impermeability of the porous medium was evolved in the topology optimization procedure to derive the geometrical configurations of the fluidic structures. Inspired by the porous medium model developed in [19], this paper implements topology optimization of fluidic flows at material interfaces by filling the porous medium on the 2-manifolds. Correspondingly, an artificial Darcy friction is added to the area force term of the surface Navier-Stokes equations.

To solve the fluidic flow problems on 2-manifolds filled with the porous medium, surface finite element methods can be used to discretize the surface Navier-Stokes equations, where a Lagrange multiplier method and a penalty technique have been developed to enforce the tangentiality constraints of the flow fields [73, 74]. Because the Lagrange multiplier method can ensure the more accurate enforcement of the tangentiality constraints of the flow fields, it is chosen to solve the surface Navier-Stokes equations. Based on the porous medium model and the surface finite element method, the topology optimization approach is formulated for the unsteady fluidic flows at material interfaces. This approach can be reduced into the forms for the steady fluidic flows at material interfaces by setting the flow fields to be independent of time.

The remaining sections of the paper are organized as follows. In Section 2, a monolithic description of the topology optimization problem for fluidic flows at material interfaces is presented. In Section 3, numerical implementation for the iterative solution of the topology optimization problem and surface finite element discretization of related partial differential equations are introduced. In Section 4, numerical examples are provided to demonstrate the developed topology optimization approach for fluidic flows on 2-manifolds. In Section 5, 6 and 7, the conclusion, acknowledgment and appendix of this paper are provided. All the mathematical descriptions are performed in the Cartesian system.

## 2 Methodology

In this section, the topology optimization problem for incompressible flows on material interfaces in terms of 2-manifolds is described by using the material distribution method.

### 2.1 Surface Navier-Stokes equations

The equations of motion of Newtonian surface fluids are formulated intrinsically on a 2-manifold of codimension one in an Euclidian space (Figure 1a). In the incompressible cases, the constitutive law of a Newtonian surface fluid is

$$\sigma_\Gamma = -p\mathbf{P} + \mu (\nabla_\Gamma \mathbf{u} + \nabla_\Gamma^T \mathbf{u}), \text{ at } \forall \mathbf{x} \in \Gamma \quad (1)$$

where  $\Gamma$  is the 2-manifold loaded with the fluid flows;  $\sigma_\Gamma$  is the Boussinesq-Scriven surface stress tensor [75, 76];  $p$  is the surface pressure;  $\mu$  is the shear viscosity of the fluid on  $\Gamma$ ; the superscript T represents the operator for the transposition of a tensor;  $\mathbf{P} = \mathbf{I} - \mathbf{n}\mathbf{n}^T$  is the normal projector on the tangential space at  $\mathbf{x} \in \Gamma$ , with  $\mathbf{x}$  denoting a node on  $\Gamma$ ;  $\mathbf{I}$  is the three-dimensional unitary tensor;  $\mathbf{n}$  is unitary normal vector of  $\Gamma$ ;  $\nabla_\Gamma$  is the tangential gradient operator. The evolution of time  $t$  from 0 to  $T$  together with the 2-manifold  $\Gamma$  defines a 3-manifold (three-dimensional

manifold), where  $T$  is the terminal time. This 3-manifold is the direct product of  $(0, T)$  and  $\Gamma$ . It is a time-space manifold, and can be expressed as

$$S := (0, T) \otimes \Gamma, \quad (2)$$

where  $\otimes$  is the operator of direct product and  $S$  is the 3-manifold sketched in Figure 1b. Based on the conservation laws of momentum and mass, the surface Navier-Stokes equations can be derived to describe the incompressible surface flows:

$$\rho \left[ \frac{\partial \mathbf{u}}{\partial t} + (\mathbf{u} \cdot \nabla_\Gamma) \mathbf{u} \right] = -\nabla_\Gamma^T p + \text{div}_\Gamma [\mu (\nabla_\Gamma \mathbf{u} + \nabla_\Gamma^T \mathbf{u})] + \mathbf{b}_\Gamma \left. \vphantom{\frac{\partial \mathbf{u}}{\partial t}} \right\} \text{ at } \forall (t, \mathbf{x}) \in S, \quad (3)$$

$$-\text{div}_\Gamma \mathbf{u} = 0$$

where  $\rho$  is the fluid density;  $\mathbf{b}_\Gamma$  is the area forces in the tangential spaces of  $\Gamma$ ;  $\text{div}_\Gamma$  is the tangential divergence operator. Because the fluid spatially flows on the 2-manifold  $\Gamma$ , the fluid velocity is vector in the tangential space of  $\Gamma$ , and it satisfies a tangential constraint of the fluid velocity:

$$\mathbf{u} \cdot \mathbf{n} = 0, \text{ at } \forall (t, \mathbf{x}) \in S. \quad (4)$$

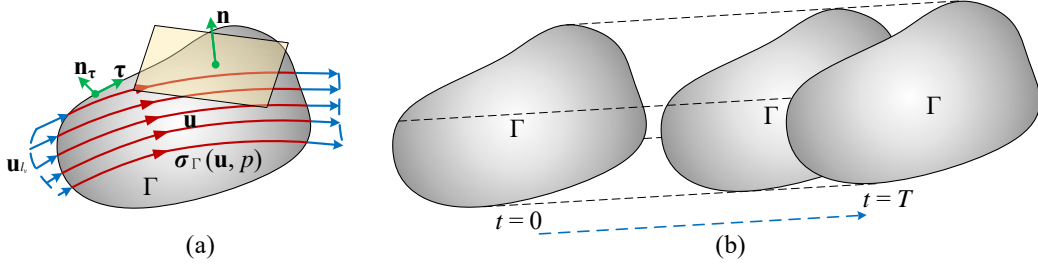


Figure 1: (a) Sketch for a surface flow on a 2-manifold  $\Gamma$ , where  $\boldsymbol{\sigma}_\Gamma$  is the Boussinesq-Scriven surface stress tensor,  $\mathbf{u}$  is the fluid velocity,  $p$  is the fluid pressure,  $\mathbf{u}_0$  is a known fluid velocity at the boundary of  $\Gamma$ ,  $\mathbf{n}$  is the unitary normal vector of  $\Gamma$ ,  $\boldsymbol{\tau}$  is the unitary tangential vector at  $\partial\Gamma$  and  $\mathbf{n}_\tau = \mathbf{n} \times \boldsymbol{\tau}$  is the outward unitary normal at  $\partial\Gamma$ ; (b) sketch for the 3-manifold  $S$  defined by the time interval  $(0, T)$  and the 2-manifold  $\Gamma$ , where  $T$  is the terminal time.

For the unsteady surface incompressible flows, an initial condition with specified spatial distribution of fluid velocity is required for equation 3, and it is expressed as

$$\mathbf{u} = \mathbf{u}_0, \text{ at } \forall (t, \mathbf{x}) \in \{0\} \otimes \Gamma \quad (5)$$

where  $\mathbf{u}_0$  is the specified distribution of fluid velocity on  $\Gamma$ . For the cases of steady flows, the initial condition is unnecessary.

To solve equation 3, fluid velocity or pressure are also required to be specified at some boundaries, interfaces or points on  $\Gamma$ . The following boundary, interface or point conditions are considered in this paper. Inlet or interfacial boundary condition with known fluid velocity is expressed as

$$\left. \begin{aligned} \mathbf{u} \cdot \mathbf{n}_\tau &= \mathbf{u}_{l_v} \cdot \mathbf{n}_\tau \\ \mathbf{u} - (\mathbf{u} \cdot \mathbf{n}_\tau) \mathbf{n}_\tau &= \mathbf{u}_{l_v} - (\mathbf{u}_{l_v} \cdot \mathbf{n}_\tau) \mathbf{n}_\tau \end{aligned} \right\} \text{ at } \forall (t, \mathbf{x}) \in (0, T) \otimes l_v, \quad (6)$$

where  $\mathbf{u}_{l_v}$  is the known distribution of fluid velocity;  $l_v$  satisfies  $l_v \subset \partial\Gamma$  when  $l_v$  is a boundary curve of  $\Gamma$ , and it satisfies  $l_v \subset \Gamma$  when  $l_v$  is an interface curve of  $\Gamma$ ;  $\mathbf{n}_\tau = \mathbf{n} \times \boldsymbol{\tau}$  is the outward unitary normal at  $\partial\Gamma$ , with  $\boldsymbol{\tau}$  representing the unitary tangential vector at  $\partial\Gamma$ . To ensure the compatibility between equation 6 and 4, the known fluid velocity  $\mathbf{u}_{l_v}$  should be a distribution satisfying  $\mathbf{u}_{l_v} \cdot \mathbf{n} = 0$ . When the known fluid velocity is  $\mathbf{0}$ , equation 6 degenerates into the no-slip boundary condition:

$$\left. \begin{aligned} \mathbf{u} \cdot \mathbf{n}_\tau &= 0 \\ \mathbf{u} - (\mathbf{u} \cdot \mathbf{n}_\tau) \mathbf{n}_\tau &= \mathbf{0} \end{aligned} \right\} \text{ at } \forall (t, \mathbf{x}) \in (0, T) \otimes l_{v0}, \quad (7)$$

where  $\mathbf{u}_{l_v}$  is equal to  $\mathbf{0}$  on  $l_{v0} \subset l_v$ , and  $l_{v0}$  is the no-slip part of the boundary curve. Open boundary condition with zero tangential stress is expressed as

$$\boldsymbol{\sigma}_\Gamma \mathbf{n}_\tau = \mathbf{0}, \text{ at } \forall (t, \mathbf{x}) \in (0, T) \otimes l_s \quad (8)$$

where  $l_s$  is the boundary satisfies  $l_s \subset \partial\Gamma$ . Point condition with known fluid pressure is expressed as

$$p = p_0, \text{ at } \forall (t, \mathbf{x}) \in (0, T) \otimes \mathcal{P} \quad (9)$$

where  $p_0$  is the known fluid pressure;  $\mathcal{P} \subset \Gamma$  is a finite point set.

The variational formulation of the surface Navier-Stokes equations is considered in the functional spaces without containing the tangential constraint of the fluid velocity as that in equation 4. The tangential constraint of the fluid velocity is imposed by using a Lagrangian multiplier method. Based on the Galerkin method, the variational formulation of surface Navier-Stokes equations can be derived as:

$$\begin{aligned}
& \text{find } \begin{cases} \mathbf{u} \in (\mathcal{H}(S))^3 \text{ with } \begin{cases} \mathbf{u} - (\mathbf{u} \cdot \mathbf{n}_\tau) \mathbf{n}_\tau = \mathbf{u}_{l_v} - (\mathbf{u}_{l_v} \cdot \mathbf{n}_\tau) \mathbf{n}_\tau, \text{ at } \forall (t, \mathbf{x}) \in (0, T) \otimes l_v \\ \mathbf{u} = \mathbf{u}_0, \text{ at } \forall (t, \mathbf{x}) \in \{0\} \otimes \Gamma \end{cases} \\ p \in \mathcal{H}(S) \text{ with } p = p_0 \text{ at } \forall (t, \mathbf{x}) \in (0, T) \otimes \mathcal{P}, \\ \lambda \in \mathcal{L}^2(S) \text{ with } \lambda = 0 \text{ at } \forall (t, \mathbf{x}) \in (0, T) \otimes l_v, \end{cases} \\
& \text{satisfying } \int_0^T \int_\Gamma \rho \left[ \frac{\partial \mathbf{u}}{\partial t} + (\mathbf{u} \cdot \nabla_\Gamma) \mathbf{u} \right] \cdot \tilde{\mathbf{u}} + \frac{\mu}{2} (\nabla_\Gamma \mathbf{u} + \nabla_\Gamma^T \mathbf{u}) : (\nabla_\Gamma \tilde{\mathbf{u}} + \nabla_\Gamma^T \tilde{\mathbf{u}}) \\
& - p \operatorname{div}_\Gamma \tilde{\mathbf{u}} + \mathbf{u} \cdot \nabla_\Gamma \tilde{p} - \mathbf{b}_\Gamma \cdot \tilde{\mathbf{u}} + \lambda (\tilde{\mathbf{u}} \cdot \mathbf{n}) + \tilde{\lambda} (\mathbf{u} \cdot \mathbf{n}) \, ds dt - \int_0^T \int_{l_v} \mathbf{u}_{l_v} \cdot \mathbf{n}_\tau \tilde{p} \, dl dt \\
& - \int_0^T \int_{\partial \Gamma \setminus l_v} \mathbf{u} \cdot \mathbf{n}_\tau \tilde{p} \, dl dt = 0, \text{ for } \forall \tilde{\mathbf{u}} \in (\mathcal{H}(S))^3, \forall \tilde{p} \in \mathcal{H}(S) \text{ and } \forall \tilde{\lambda} \in \mathcal{L}^2(S)
\end{aligned} \tag{10}$$

where  $\lambda$  is the Lagrange multiplier used to impose the tangential constraint of the fluid velocity;  $\mathcal{H}(S)$  and  $\mathcal{L}^2(S)$  are the first order Sobolev space and second order Lebesgue space defined on  $S$ , respectively;  $\tilde{\mathbf{u}}$ ,  $\tilde{p}$  and  $\tilde{\lambda}$  are the test functions of  $\mathbf{u}$ ,  $p$  and  $\lambda$ , respectively. **The Lagrangian multiplier used to impose the tangential constraint of the fluid velocity plays the role of a distributed force in the normal direction of the 2-manifold. When the fluidic particles cooperatively move on the 2-manifold, the centrifugal, Coriolis and Euler forces are induced by the non-zero distribution of the curvature of the 2-manifold. Those forces have the components in the normal direction of the 2-manifold, i.e., the normal components of the centrifugal, Coriolis and Euler forces. These normal components of the forces are cancelled out by the distributed force corresponding to the Lagrangian multiplier, to ensure the satisfaction of the tangential constraint of the fluid velocity.**

The above surface Navier-Stokes equations and their variational formulation are introduced for unsteady flows. For the steady flows, the time dependence is casted off by removing the local-derivative term  $\partial \mathbf{u} / \partial t$  from equation 3. Sequentially, the time-space 3-manifold  $S$  in equation 2 degenerates into the spacial 2-manifold  $\Gamma$ ; the initial condition in equation 5 is unnecessary; all the time dependence can be removed from the tangential constraint in equations 4 and boundary, interface and point conditions in equations 6, 8 and 9; the time integration of the variational formulation in equation 10 can be removed; and the relevant functions will be located in the first order Sobolev space  $\mathcal{H}(\Gamma)$  and Lebesgue space  $\mathcal{L}^2(\Gamma)$  instead of  $\mathcal{H}(S)$  and  $\mathcal{L}^2(S)$ .

## 2.2 Porous medium model

For topology optimization of flows on 2-manifolds, the porous medium based models are utilized inheritically. In this model, an artificial Darcy friction is added into the area force term of the surface Navier-Stokes equations in equation 3 defined on a 2-manifold filled with surface porous medium. The artificial Darcy friction in the surface porous medium is assumed to be proportional to the fluid velocity [19, 20], and it is expressed as

$$\mathbf{b}_a = -\alpha \mathbf{u}, \tag{11}$$

where  $\alpha$  is the impermeability of the porous medium. The material interpolation is implemented on the impermeability [19]:

$$\alpha(\gamma_p) = \alpha_f + (\alpha_s - \alpha_f) q \frac{1 - \gamma_p}{q + \gamma_p}, \tag{12}$$

where  $\alpha_s$  and  $\alpha_f$  are the impermeability of the solid and fluid phases, respectively;  $q$  is the parameter used to tune the convexity of this interpolation;  $\gamma_p$  valued continuously in  $[0, 1]$  is the material density of the fluidic structure defined on  $\Gamma$ . The lower bound 0 and upper bound 1 of  $\gamma_p$  represent the solid and fluid phases, respectively. For the fluid phase, the impermeability of a fluid is zeros, hence  $\alpha_f = 0$ . For the solid phase,  $\alpha_s$  should be infinite theoretically; numerically, a finite value much larger than the fluid density  $\rho$  is chosen for it, to ensure the stability of the numerical implementation and approximate the solid phase with enough accuracy. Based on numerical tests,  $q$  is valued as 1, and  $\alpha_s$  is chosen as  $10^4 \rho$  to satisfy  $\alpha_s \gg \rho$ .

After adding the artificial Darcy friction, the area force term in the surface Navier-Stokes equations can be divided into two parts, i.e., the artificial Darcy friction and physical area force:

$$\mathbf{b}_\Gamma = -\alpha \mathbf{u} + \chi \mathbf{b}_p, \quad (13)$$

where  $\mathbf{b}_p$  is the physical area force, and it can include the gravity, centrifugal force along with Coriolis and Euler forces in a rotating frame, electromagnetic forces, etc;  $\chi$  is a penalizing factor imposed on  $\mathbf{b}_p$ . It has been specified that the physical forces can enlarge fluid velocity in the regions with high impermeability; this can result in the invalidity of the porous medium based model for topology optimization of flow problems [35]. To solve this problem, a penalization is implemented by multiplying the physical force  $\mathbf{b}_p$  with the penalizing factor expressed as

$$\chi(\gamma_p) = \chi_{\min} + (\chi_{\max} - \chi_{\min}) q \frac{1 - \gamma_p}{q + \gamma_p}, \quad (14)$$

where  $\chi_{\min} = 0$  and  $\chi_{\max} = 1$  are the minimal and maximal values of  $\chi$ , respectively. The affect of the penalization is to achieve the physical retrieval by gradually removing the physical force from solid phase and keeping its existence in the liquid phase. Then, the problem on the invalidity of the porous medium based model can be avoided, when the physical force exists.

### 2.3 Design variable for material density

The fluidic structure is immutable in flow problems, although the fluid velocity and pressure can vary along with time in the unsteady flow. The material density of the fluidic structure is independent of time. It can be derived by sequentially implementing surface-PDE filter and threshold projection operations on a design variable, which is independent of time and defined on the 2-manifold  $\Gamma$  and valued continuously in  $[0, 1]$ . Inspired by the PDE filter developed in [77], the surface-PDE filter for the design variable is implemented by solving the following PDE defined on the 2-manifold [66]:

$$\begin{cases} -\operatorname{div}_\Gamma(r_f^2 \nabla_\Gamma \gamma_f) + \gamma_f = \gamma, & \text{at } \forall \mathbf{x} \in \Gamma \\ \mathbf{n}_\tau \cdot \nabla_\Gamma \gamma_f = 0, & \text{at } \forall \mathbf{x} \in \partial\Gamma \end{cases}, \quad (15)$$

where  $\gamma$  is the design variable;  $\gamma_f$  is the filtered design variable. The threshold projection of the filtered design variable is [78, 79]

$$\gamma_p = \frac{\tanh(\beta\xi) + \tanh(\beta(\gamma_f - \xi))}{\tanh(\beta\xi) + \tanh(\beta(1 - \xi))}, \quad (16)$$

where  $r_f$  is the filter radius and it is constant;  $\beta$  and  $\xi$  are the parameters for the threshold projection, with values chosen based on numerical experiments [79]. The method of deriving a material density by sequentially implementing the surface-PDE filter and threshold projection on a design variable can effectively remove the gray regions and control the feature size of a derived fluidic structure.

The variational formulation of the surface-PDE filter is considered in the first order Sobolev space defined on  $\Gamma$ . Based on the Galerkin method, the variational formulation of the surface-PDE filter can be derived as:

$$\begin{aligned} &\text{find } \gamma_f \in \mathcal{H}(\Gamma) \text{ for } \gamma \in \mathcal{L}^2(\Gamma), \text{ satisfying} \\ &\int_\Gamma r_f^2 \nabla_\Gamma \gamma_f \cdot \nabla_\Gamma \tilde{\gamma}_f + \gamma_f \tilde{\gamma}_f - \gamma \tilde{\gamma}_f \, ds = 0, \text{ for } \forall \tilde{\gamma}_f \in \mathcal{H}(\Gamma) \end{aligned} \quad (17)$$

where  $\tilde{\gamma}_f$  is the test function of  $\gamma_f$ .

### 2.4 Topology optimization problem

Based on the introduction of the surface Navier-Stokes equations and porous medium based model, a general form can be constructed for the topology optimization problem of surface

$$\begin{aligned} & \text{find } \gamma : \Gamma \mapsto [0, 1] \text{ to minimize } \frac{J}{J_0} \text{ with} \\ J &= \int_0^T \int_{\Gamma} A(\mathbf{u}, \nabla_{\Gamma} \mathbf{u}, p; \gamma_p) \, \mathrm{d}s \mathrm{d}t + \int_0^T \int_{\partial \Gamma} B(\mathbf{u}, p) \, \mathrm{d}l \mathrm{d}t + \int_{\Gamma} C(\mathbf{u}; \gamma_p) \big|_{t=T} \, \mathrm{d}s, \end{aligned}$$
$$\left\{ \begin{array}{l} \rho \left[ \frac{\partial \mathbf{u}}{\partial t} + (\mathbf{u} \cdot \nabla_{\Gamma}) \mathbf{u} \right] = -\nabla_{\Gamma}^T p + \operatorname{div}_{\Gamma} \left[ \mu \left( \nabla_{\Gamma} \mathbf{u} + \nabla_{\Gamma}^T \mathbf{u} \right) \right] - \alpha \mathbf{u} + \chi \mathbf{b}_p \\ -\operatorname{div}_{\Gamma} \mathbf{u} = 0 \\ \mathbf{u} \cdot \mathbf{n} = 0 \end{array} \right\} \text{ at } \forall (t, \mathbf{x}) \in S,$$

$$\left\{ \begin{array}{l} \alpha(\gamma_p) = \alpha_f + (\alpha_s - \alpha_f) q \frac{1 - \gamma_p}{q + \gamma_p} \\ \chi(\gamma_p) = \chi_{\max} + (\chi_{\min} - \chi_{\max}) q \frac{1 - \gamma_p}{q + \gamma_p} \\ -\operatorname{div}_{\Gamma} (r_f^2 \nabla_{\Gamma} \gamma_f) + \gamma_f = \gamma, \text{ at } \forall \mathbf{x} \in \Gamma \\ \mathbf{n}_{\tau} \cdot \nabla_{\Gamma} \gamma_f = 0, \text{ at } \forall \mathbf{x} \in \partial \Gamma \end{array} \right.,$$

$$\gamma_p = \frac{\tanh(\beta \xi) + \tanh(\beta(\gamma_f - \xi))}{\tanh(\beta \xi) + \tanh(\beta(1 - \xi))}$$

$$|v - v_0| \leq 10^{-3} \text{ with } v = \frac{1}{|\Gamma|} \int_{\Gamma} \gamma_p \, ds \quad (\text{Area constraint})$$

$$(18)$$

The topology optimization problem in equation 18 is formulated for unsteady flows. For steady flows, reduction can be implemented by setting the related variables to be independent of time. The time integration in the optimization objective  $J$  is casted off, and the surface integration term about  $C$  defined at the terminal time  $t = T$  is unnecessary; the surface Navier-Stokes equations in the constraints are degenerated into the stationary ones as discussed in Section 2.1.

The topology optimization problem in equation 18 can be solved by using a gradient information-based iterative procedure, where the adjoint sensitivities are used to determine the relevant gradient information. The adjoint analysis is implemented for the optimization objective and area constraint to derive their adjoint sensitivities.

$$\delta J = -T \int_{\Gamma} \gamma_{fa} \delta \gamma \, ds, \quad (19)$$

Variational formulation for the adjoint equations of the surface Navier-Stokes equations is

$$\begin{aligned}
& \text{find } \begin{cases} \mathbf{u}_a \in (\mathcal{H}(S))^3 \text{ with } \begin{cases} \mathbf{u}_a - (\mathbf{u}_a \cdot \mathbf{n}_\tau) \mathbf{n}_\tau = \mathbf{0}, \text{ at } \forall (t, \mathbf{x}) \in (0, T) \otimes l_v \\ \mathbf{u}_a = -\frac{1}{\rho} \frac{\partial C}{\partial \mathbf{u}}, \text{ at } \forall (t, \mathbf{x}) \in \{T\} \otimes \Gamma \end{cases} \\ p_a \in \mathcal{H}(S) \text{ with } p_a = 0 \text{ at } \forall (t, \mathbf{x}) \in (0, T) \otimes \mathcal{P}, \\ \lambda_a \in \mathcal{L}^2(S) \text{ with } \lambda_a = 0 \text{ at } \forall (t, \mathbf{x}) \in (0, T) \otimes l_v, \end{cases} \\
& \text{satisfying } \int_0^T \int_\Gamma \frac{\partial A}{\partial \mathbf{u}} \cdot \tilde{\mathbf{u}}_a + \frac{\partial A}{\partial \nabla_\Gamma \mathbf{u}} : \nabla_\Gamma \tilde{\mathbf{u}}_a + \frac{\partial A}{\partial p} \tilde{p}_a - \rho \frac{\partial \mathbf{u}_a}{\partial t} \cdot \tilde{\mathbf{u}}_a \\
& + \rho [(\tilde{\mathbf{u}}_a \cdot \nabla_\Gamma) \mathbf{u} + (\mathbf{u} \cdot \nabla_\Gamma) \tilde{\mathbf{u}}_a] \cdot \mathbf{u}_a + \frac{\mu}{2} (\nabla_\Gamma \mathbf{u}_a + \nabla_\Gamma^T \mathbf{u}_a) : (\nabla_\Gamma \tilde{\mathbf{u}}_a + \nabla_\Gamma^T \tilde{\mathbf{u}}_a) \\
& + \left( \alpha \mathbf{I} - \chi \frac{\partial \mathbf{b}_p}{\partial \mathbf{u}} \right) \mathbf{u}_a \cdot \tilde{\mathbf{u}}_a + \mathbf{u}_a \cdot \nabla_\Gamma \tilde{p}_a - p_a \text{div}_\Gamma \tilde{\mathbf{u}}_a + (\tilde{\lambda}_a \mathbf{u}_a + \lambda_a \tilde{\mathbf{u}}_a) \cdot \mathbf{n} \, ds dt \\
& - \int_0^T \int_{\partial \Gamma} \left( \mathbf{u}_a \cdot \mathbf{n}_\tau - \frac{\partial B}{\partial p} \right) \tilde{p}_a \, dl dt + \int_0^T \int_{\partial \Gamma \setminus l_v} \frac{\partial B}{\partial \mathbf{u}} \cdot \tilde{\mathbf{u}}_a \, dl dt = 0, \\
& \text{for } \forall \tilde{\mathbf{u}}_a \in (\mathcal{H}(S))^3, \forall \tilde{p}_a \in \mathcal{L}^2(S) \text{ and } \forall \tilde{\lambda}_a \in \mathcal{L}^2(S)
\end{aligned} \tag{20}$$

where  $\mathbf{u}_a$ ,  $p_a$  and  $\lambda_a$  are the adjoint variables of  $\mathbf{u}$ ,  $p$  and  $\lambda$ , respectively;  $\tilde{\mathbf{u}}_a$ ,  $\tilde{p}_a$  and  $\tilde{\lambda}_a$  are the test functions of  $\mathbf{u}_a$ ,  $p_a$  and  $\lambda_a$ , respectively.

Variational formulation of the adjoint equation of the surface-PDE filter is

$$\begin{aligned}
& \text{find } \gamma_{fa} \in \mathcal{H}(\Gamma), \text{ satisfying} \\
& \frac{1}{T} \int_0^T \int_\Gamma \left( \frac{\partial A}{\partial \gamma_p} + \frac{\partial \alpha}{\partial \gamma_p} \mathbf{u} \cdot \mathbf{u}_a - \frac{\partial \chi}{\partial \gamma_p} \mathbf{b}_p \cdot \mathbf{u}_a \right) \frac{\partial \gamma_p}{\partial \gamma_f} \tilde{\gamma}_{fa} \, ds dt + \frac{1}{T} \int_\Gamma \frac{\partial C}{\partial \gamma_p} \Big|_{t=T} \frac{\partial \gamma_p}{\partial \gamma_f} \tilde{\gamma}_{fa} \, ds \\
& + \int_\Gamma r_f^2 \nabla_\Gamma \gamma_{fa} \cdot \nabla_\Gamma \tilde{\gamma}_{fa} + \gamma_{fa} \tilde{\gamma}_{fa} \, ds = 0, \text{ for } \forall \tilde{\gamma}_{fa} \in \mathcal{H}(\Gamma)
\end{aligned} \tag{21}$$

where  $\tilde{\gamma}_{fa}$  is the test function of  $\gamma_{fa}$ .

The adjoint sensitivity of the area fraction  $v$  can be derived as

$$\delta v = -\frac{1}{|\Gamma|} \int_\Gamma \gamma_{fa} \delta \gamma \, ds, \tag{22}$$

where  $\gamma_{fa}$  can be derived from the following variational formulation for the adjoint equation of the surface-PDE filter:

$$\begin{aligned}
& \text{find } \gamma_{fa} \in \mathcal{H}(\Gamma), \text{ satisfying} \\
& \int_\Gamma \frac{\partial \gamma_p}{\partial \gamma_f} \tilde{\gamma}_{fa} + r_f^2 \nabla_\Gamma \gamma_{fa} \cdot \nabla_\Gamma \tilde{\gamma}_{fa} + \gamma_{fa} \tilde{\gamma}_{fa} \, ds = 0, \text{ for } \forall \tilde{\gamma}_{fa} \in \mathcal{H}(\Gamma).
\end{aligned} \tag{23}$$

The adjoint analysis is implemented on the topology optimization problem for unsteady flows. For steady flows, It can be changed into the one for steady flows by implementing the following reduction. For the steady-flow cases, reduction can be implemented directly based on the time-independence of the fluidic velocity and pressure, with casting off the surface integration term about  $C$  defined at the terminal time  $t = T$  and degenerating the functional spaces into the ones defined on  $\Gamma$  instead of  $S$ .

After the derivation of the adjoint sensitivities in equation 19 and 23, the design variable  $\gamma$  can be evolved iteratively to inversely design a fluidic structure on a 2-manifold.

### 3 Numerical implementation

After adjoint analysis, the topology optimization problem in equation 18 is solved by using the numerical approach described as follows.

#### 3.1 Iterative procedure

A topology optimization procedure is implemented as outlined by the pseudo codes in Table 1, where a loop is included for the iterative solution of the topology optimization problem in equation 18. The surface finite element method is utilized to solve the variational formulations of the relevant PDEs and adjoint equations [81].

In the iterative procedure, the projection parameter  $\beta$  with the initial value 1 is doubled after every 30 iterations; the loop is stopped when the maximal iteration number is reached, or if the averaged variation of the design objective in continuous 5 iterations and residual of the area constraint are simultaneously less than the specified tolerance  $10^{-3}$  chosen to be much less than 1. The design variable is updated by using the method of moving asymptotes [82].

---

**Algorithm 1:** iterative solution of equation 18

---

Set  $\mathbf{u}_0, \mathbf{u}_{t_v}, p_0, \rho, \mu$  and  $v_0$ ;

Set  $\begin{cases} \gamma \leftarrow v_0 \\ n_{\max} \leftarrow 315 \\ n_i \leftarrow 1 \\ \xi \leftarrow 0.5 \\ \beta \leftarrow 1 \end{cases}$  and  $\begin{cases} \alpha_{\min} \leftarrow 0 \\ \alpha_{\max} \leftarrow 10^4 \rho \\ \chi_{\min} \leftarrow 0 \\ \chi_{\max} \leftarrow 1 \\ q \leftarrow 10^{-1} \end{cases}$  ;

**loop**

Solve equation 17 to derive  $\gamma_f$  by filtering  $\gamma$ ;

Project  $\gamma_f$  to derive  $\gamma_p$  and compute  $v$ ;

Solve  $\mathbf{u}, p$  and  $\lambda$  from equation 10, and evaluate  $J/J_0$ ;

Solve  $\mathbf{u}_a, p_a, \lambda_a$  and  $\gamma_{fa}$  from equation 20 and 21;

Evaluate  $\delta J$  from equation 19;

Solve  $\gamma_{fa}$  from equation 23;

Evaluate  $\delta v$  from equation 22;

Update  $\gamma$  based on  $\delta J$  and  $\delta v$ ;

**if**  $\text{mod}(n_i, 30) == 0$

$\beta \leftarrow 2\beta$ ;

**end if**

**if**  $(n_i == n_{\max})$  or  $\begin{cases} \beta == 2^{10} \\ \frac{1}{5} \sum_{m=0}^4 |J_{n_i} - J_{n_i-m}| / J_0 \leq 10^{-3} \\ |v - v_0| \leq 10^{-3} \end{cases}$

break;

**end if**

$n_i \leftarrow n_i + 1$

**end loop**

---

Table 1: Pseudo codes used to solve topology optimization problem of fluidic flows on 2-manifolds. In the iterative solution loop for the topology optimization problem in equation 18,  $n_i$  is the loop-index,  $n_{\max}$  is the maximal value of  $n_i$ ,  $J_{n_i}$  is the value of  $J$  in the  $n_i$ -th iteration, and  $\text{mod}$  is the operator used to take the remainder.



### 3.2 Surface finite element solution

To solve the variational formulations of the PDE constraints and their adjoint equations, a surface finite element method is utilized [81]. In the surface finite element method, the 2-manifold  $\Gamma$  is approximated by a discrete surface, the union of finite elements, which are finitely many non-degenerate  $n$ -simplices in  $\mathbb{R}^3$  with  $n$  denoting the number of the finite elements. This discrete surface is denoted as

$$\Gamma_h = \bigcup_{E \in \mathcal{E}_h} E, \quad (24)$$

where  $\Gamma_h$  is the discrete surface;  $\mathcal{E}_h$  is the  $n$ -simplices;  $E$  is an element of  $\mathcal{E}_h$ ; the subscript  $h$  denotes the feature size of the finite elements, and it is defined as  $h = \max_{E \in \mathcal{E}_h} h(E)$  with  $h(E)$  representing the size of the finite element  $E$ . The elementization  $\mathcal{E}_h$  is the polygonalization of  $\Gamma$ , where the elements are usually quadrangles or triangles. In this paper, elementization of quadrangles are used (Figure 2). For functions  $f : \Gamma_h \mapsto \mathbb{R}$  and  $\mathbf{v} : \Gamma_h \mapsto \mathbb{R}^3$ , the tangential gradient and divergence on the discrete surface are

$$\begin{cases} \nabla_{\Gamma_h} f = \mathbf{P}_h \nabla f \\ \operatorname{div}_{\Gamma_h} \mathbf{v} = \operatorname{tr}(\nabla_{\Gamma_h} \mathbf{v}) = \operatorname{tr}((\nabla \mathbf{v}) \mathbf{P}_h) \end{cases}, \quad (25)$$

where  $\mathbf{P}_h = \mathbf{I} - \mathbf{n}_h \mathbf{n}_h^T$  is the normal projector on the tangential space of  $\Gamma_h$ ;  $\mathbf{n}_h$  is the unitary normal vector on  $\Gamma_h$ .

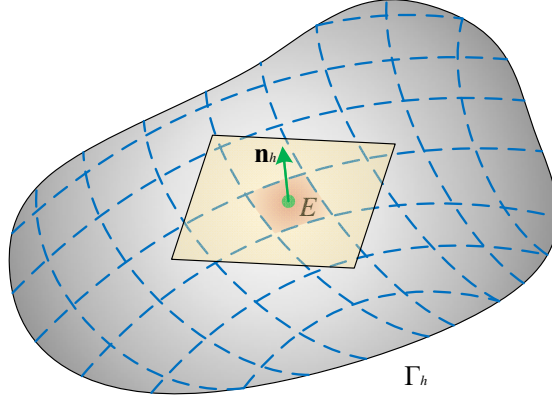


Figure 2: Sketch for the elementization  $\mathcal{E}_h$  of  $\Gamma$  by using quadrangular elements, where  $\Gamma_h$  is the discrete surface,  $E$  is an element of  $\mathcal{E}_h$  and  $\mathbf{n}_h$  is the unitary normal vector on  $\Gamma_h$ .

To ensure the well-posedness of the variational formulations of the surface Navier-Stokes equations and their adjoint equations (equation 10 and 20), Taylor-Hood elements are used to satisfy the *inf-sup* condition [83]. To ensure the efficiency and positivity of the design variable, linear elements are used to interpolate and solve the variational formulations of the surface-PDE filter and its adjoint equation (equation 17, 21 and 23). The finite element nodes of a Taylor-Hood element and a linear element of the elementization  $\mathcal{E}_h$  have been sketched in Figure 3. Therefore, quadratic elements are used for the fluidic velocity  $\mathbf{u}$ , Lagrangian multiplier  $\lambda$  and their adjoint variables; the corresponding finite element space is

$$\mathcal{S}_h^{(2)} = \left\{ \phi_h \in C^0(\Gamma_h) : \phi_h(\mathbf{x})|_{\mathbf{x} \in E} \text{ is a quadratic affine for } \forall E \in \mathcal{E}_h \right\}, \quad (26)$$

where  $C^0(\Gamma_h)$  is the space of the continuous functions defined on  $\Gamma_h$ . This space can be spanned by the nodal basis  $\{\psi_1^{(2)}, \psi_2^{(2)}, \dots, \psi_{N_2}^{(2)}\}$  satisfying

$$\left. \begin{aligned} \psi_i^{(2)} &\in \mathcal{S}_h^{(2)} \\ \psi_i^{(2)}(\mathbf{x}_j^{(2)}) &= \delta_{ij} \end{aligned} \right\} \text{ for } i, j = 1, 2, \dots, N_2 \quad (27)$$

where  $N_2$  is the number of interpolation nodes;  $\{\mathbf{x}_j^{(2)} : j = 1, 2, \dots, N_2\} \subset \Gamma$  denotes the nodes for quadratic interpolation on the elementization  $\mathcal{E}_h$ ;  $\delta_{ij}$  is the Kronecker symbol.  $\delta_{ij}$  is 1 when  $i = j$  is satisfied; or else, it is 0. Linear elements are used for the fluidic pressure  $p$ , design variable  $\gamma$ , filtered design variable  $\gamma_f$  and their adjoint variables; the corresponding finite element space is

$$\mathcal{S}_h^{(1)} = \left\{ \phi_h \in C^0(\Gamma_h) : \phi_h(\mathbf{x})|_{\mathbf{x} \in E} \text{ is a linear affine for } \forall E \in \mathcal{E}_h \right\}, \quad (28)$$

where  $\phi_h$  is linear when  $\mathcal{E}_h$  is the triangulation of  $\Gamma$ , and it is bilinear when  $\mathcal{E}_h$  is the quadrangulation of  $\Gamma$ . This space can be spanned by the nodal basis  $\{\psi_1^{(1)}, \psi_2^{(1)}, \dots, \psi_{N_1}^{(1)}\}$  satisfying

$$\left. \begin{aligned} \psi_i^{(1)} &\in \mathcal{S}_h^{(1)} \\ \psi_i^{(1)}(\mathbf{x}_j^{(1)}) &= \delta_{ij} \end{aligned} \right\} \text{ for } i, j = 1, 2, \dots, N_1 \quad (29)$$

where  $N_1$  is the number of interpolation nodes;  $\{\mathbf{x}_j^{(1)} : j = 1, 2, \dots, N_1\} \subset \Gamma$  denotes the nodes for linear or bilinear interpolation on the elementization  $\mathcal{E}_h$ . For a quadrangle element,  $N_2$  in equation 27 and  $N_1$  in equation 29 are 9 and 4, respectively.

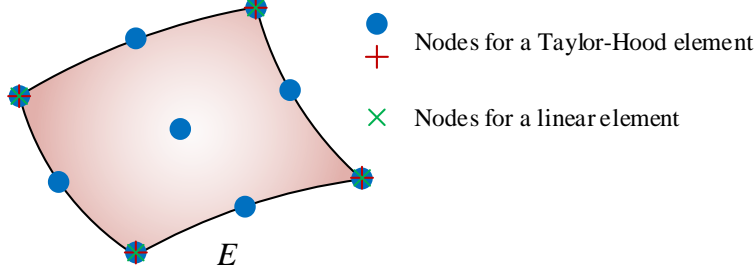


Figure 3: Sketch for the nodes of a Taylor-Hood element and a linear element.

To discretize the time derivative terms of the variational formulations, the backward differentiation formula (BDF) is utilized [84]. Here, the  $m$ -step BDF is adopted with  $m \leq 6$  with  $m$  representing the step number of the BDF algorithm, because the methods with  $m > 6$  are not zero-stable [85].

### 3.2.1 Discretization of variational formulation in equation 17

Based on the surface finite element method, the variational formulation (equation 17) for the surface-PDE filter is transformed to be defined on  $\Gamma_h$  as:

$$\begin{aligned} &\text{find } \gamma_{f,h} \in \mathcal{S}_h^{(1)}, \text{ satisfying} \\ &\int_{\Gamma_h} r_f^2 \nabla_{\Gamma_h} \gamma_{f,h} \cdot \nabla_{\Gamma_h} \tilde{\gamma}_{f,h} + \gamma_{f,h} \tilde{\gamma}_{f,h} - \gamma_h \tilde{\gamma}_{f,h} \, ds = 0, \text{ for } \forall \tilde{\gamma}_{f,h} \in \mathcal{S}_h^{(1)} \end{aligned} \quad (30)$$

where  $\gamma_h$  and  $\gamma_{f,h}$  are the design variable and its filtered counterpart on  $\Gamma_h$ .

Based on the nodal basis  $\{\psi_1^{(1)}, \psi_2^{(1)}, \dots, \psi_{N_1}^{(1)}\}$  for  $\mathcal{S}_h^{(1)}$ ,  $\gamma_h$  and  $\gamma_{f,h}$  have the following form:

$$\left. \begin{aligned} \gamma_h &= \sum_{i=1}^{N_1} \Upsilon_{h,i} \psi_i^{(1)}(\mathbf{x}) \\ \gamma_{f,h} &= \sum_{i=1}^{N_1} \Upsilon_{f,h,i} \psi_i^{(1)}(\mathbf{x}) \end{aligned} \right\} \text{ at } \forall \mathbf{x} \in \Gamma_h, \quad (31)$$

where  $\Upsilon_{h,i}$  and  $\Upsilon_{f,h,i}$  are the nodal variables of  $\gamma_h$  and  $\gamma_{f,h}$ , respectively. By substituting equation 31 into equation 30, and using the nodal basis of  $\mathcal{S}_h^{(1)}$  as the test functions, a linear system can be derived based on the assembly rule of stiffness matrix:

$$(\mathbf{K} + \mathbf{N}) \mathbf{\Upsilon}_f = \mathbf{N} \mathbf{\Upsilon}, \quad (32)$$

where  $\mathbf{\Upsilon}_f$  and  $\mathbf{\Upsilon}$  are the discrete counterparts of  $\gamma_{f,h}$  and  $\gamma_h$ , respectively. The correspondences between the matrixes in equation 32 and terms in equation 31 are provided in equation 60 of Appendix 7.2. The variational formulation in equation 17 can be solved by using a PARDISO solver [86].

### 3.2.2 Discretization of variational formulation in equation 10

Based on the surface finite element method and  $m$ -step BDF schemes, the variational formulation (equation 10) for the surface Navier-Stokes equations is transformed to be defined on  $\Gamma_h$  as:

for  $n = 1, 2, \dots, N_t$

$$\begin{aligned} \text{find } & \begin{cases} \mathbf{u}_h^{(n)} \in (\mathcal{S}_h^{(2)})^3 \text{ with } \begin{cases} \mathbf{u}_h^{(n)} - (\mathbf{u}_h^{(n)} \cdot \mathbf{n}_{\tau,h}) \mathbf{n}_{\tau,h} = \mathbf{u}_{l_v} - (\mathbf{u}_{l_v} \cdot \mathbf{n}_{\tau,h}) \mathbf{n}_{\tau,h} \text{ at } t = n\Delta t, \forall \mathbf{x} \in l_{v,h} \\ \mathbf{u}_h^{(0)} = \mathbf{u}_0 \text{ at } \forall \mathbf{x} \in \Gamma_h \end{cases} \\ p_h^{(n)} \in \mathcal{S}_h^{(1)} \text{ with } p_h^{(n)} = p_0 \text{ at } t = n\Delta t, \forall \mathbf{x} \in \mathcal{P}_h, \\ \lambda_h^{(n)} \in \mathcal{S}_h^{(2)} \text{ with } \lambda_h^{(n)} = 0 \text{ at } t = n\Delta t, \forall \mathbf{x} \in l_{v,h}, \end{cases} \\ \text{satisfying } & \int_{\Gamma_h} \rho \frac{\theta_m \mathbf{u}_h^{(n)} - \mathbf{u}_{h,m}^{(n-1)}}{\Delta t} \cdot \tilde{\mathbf{u}}_h + \rho \left[ (\mathbf{u}_h^{(n)} \cdot \nabla_{\Gamma_h}) \mathbf{u}_h^{(n)} \right] \cdot \tilde{\mathbf{u}}_h \\ & + \frac{\mu}{2} \left( \nabla_{\Gamma_h} \mathbf{u}_h^{(n)} + \nabla_{\Gamma_h}^T \mathbf{u}_h^{(n)} \right) : \left( \nabla_{\Gamma_h} \tilde{\mathbf{u}}_h + \nabla_{\Gamma_h}^T \tilde{\mathbf{u}}_h \right) - p_h^{(n)} \operatorname{div}_{\Gamma_h} \tilde{\mathbf{u}}_h + \mathbf{u}_h^{(n)} \cdot \nabla_{\Gamma_h} \tilde{p}_h \\ & + \left( \alpha_h \mathbf{u}_h^{(n)} - \chi_h \mathbf{b}_{p,h}^{(n)} \right) \cdot \tilde{\mathbf{u}}_h + \lambda_h^{(n)} (\tilde{\mathbf{u}}_h \cdot \mathbf{n}_h) + \tilde{\lambda}_h \left( \mathbf{u}_h^{(n)} \cdot \mathbf{n}_h \right) \, ds - \int_{l_{v,h}} \mathbf{u}_{l_v} \cdot \mathbf{n}_{\tau,h} \tilde{p}_h \, dl \\ & - \int_{\partial \Gamma_h \setminus l_{v,h}} \mathbf{u}_h^{(n)} \cdot \mathbf{n}_{\tau,h} \tilde{p}_h \, dl = 0, \text{ for } \forall \tilde{\mathbf{u}}_h \in (\mathcal{S}_h^{(2)})^3, \forall \tilde{p}_h \in \mathcal{S}_h^{(1)} \text{ and } \tilde{\lambda}_h \in \mathcal{S}_h^{(2)} \end{aligned} \quad (33)$$

where  $n$  is the time step number, and it is used as the superscript of the relevant variables and functions to denote the time step; the time domain  $(0, T)$  is divided into  $N_t$  sections with the time-step length of  $\Delta t = T/N_t$ , respectively; the time-step number  $N_t$  is chosen to be large enough to ensure the numerical stability and accuracy;  $\mathbf{u}_h^{(n)}$ ,  $p_h^{(n)}$  and  $\lambda_h^{(n)}$  are the fluidic velocity, pressure and Lagrangian multiplier on  $\Gamma_h$  at time  $t = n\Delta t$ , respectively;  $\tilde{\mathbf{u}}_h$ ,  $\tilde{p}_h$  and  $\tilde{\lambda}_h$  are the test functions of  $\mathbf{u}_h^{(n)}$ ,  $p_h^{(n)}$  and  $\lambda_h^{(n)}$ , respectively;  $\alpha_h$  and  $\chi_h$  are the artificial impermeability and penalization factor on  $\Gamma_h$ , respectively;  $l_{v,h}$  and  $\mathcal{P}_h$  are the discrete counterparts of  $l_v$  and  $\mathcal{P}$ , respectively; for the  $m$ -step BDF schemes, the values of the parameter  $\theta_m$  and expression of  $\mathbf{u}_{h,m}^{(n-1)}$  determined by the linear combination of  $\{\mathbf{u}_h^{(n-1)}, \mathbf{u}_h^{(n-2)}, \dots, \mathbf{u}_h^{(n-m)}\}$  with  $n - m = 0$  are provided in Appendix 7.1.

The discretized variational formulation of the surface Navier-Stokes equations (equation 33) is nonlinear because of the convection term  $\rho \left[ (\mathbf{u}_h^{(n)} \cdot \nabla_{\Gamma_h}) \mathbf{u}_h^{(n)} \right] \cdot \tilde{\mathbf{u}}_h$ . Newton iteration turns out to be a natural approach to solve it based on the perturbation-based linearization [83]. Given the iterate  $(\mathbf{u}_{h,k}^{(n)}, p_{h,k}^{(n)}, \lambda_{h,k}^{(n)})$  with the subscript  $k$  representing the iteration number of the Newton iteration, the computing can be started from the residuals associated with the variational

$$\text{formulation in equation 33. With } \begin{cases} \mathbf{u}_h^{(n)} = \mathbf{u}_{h,k}^{(n)} + \delta \mathbf{u}_{h,k}^{(n)} \\ p_h^{(n)} = p_{h,k}^{(n)} + \delta p_{h,k}^{(n)} \\ \lambda_h^{(n)} = \lambda_{h,k}^{(n)} + \delta \lambda_{h,k}^{(n)} \end{cases}, \text{ the corrections } \begin{cases} \delta \mathbf{u}_{h,k}^{(n)} \in (\mathcal{S}_h^{(2)})^3 \\ \delta p_{h,k}^{(n)} \in \mathcal{S}_h^{(1)} \\ \delta \lambda_{h,k}^{(n)} \in \mathcal{S}_h^{(2)} \end{cases}$$

satisfy

$$\begin{aligned} & \int_{\Gamma_h} \rho \frac{\theta_m}{\Delta t} \delta \mathbf{u}_{h,k}^{(n)} \cdot \tilde{\mathbf{u}}_h + \rho \left[ (\mathbf{u}_{h,k}^{(n)} \cdot \nabla_{\Gamma_h}) \delta \mathbf{u}_{h,k}^{(n)} \right] \cdot \tilde{\mathbf{u}}_h + \rho \left[ (\delta \mathbf{u}_{h,k}^{(n)} \cdot \nabla_{\Gamma_h}) \mathbf{u}_{h,k}^{(n)} \right] \cdot \tilde{\mathbf{u}}_h \\ & + \frac{\mu}{2} \left( \nabla_{\Gamma_h} \delta \mathbf{u}_{h,k}^{(n)} + \nabla_{\Gamma_h}^T \delta \mathbf{u}_{h,k}^{(n)} \right) : \left( \nabla_{\Gamma_h} \tilde{\mathbf{u}}_h + \nabla_{\Gamma_h}^T \tilde{\mathbf{u}}_h \right) \\ & - \delta p_{h,k}^{(n)} \operatorname{div}_{\Gamma_h} \tilde{\mathbf{u}}_h + \delta \mathbf{u}_{h,k}^{(n)} \cdot \nabla_{\Gamma_h} \tilde{p}_h + \left( \alpha_h \delta \mathbf{u}_{h,k}^{(n)} - \chi_h \frac{\partial \mathbf{b}_{p,h}^{(n)}}{\partial \mathbf{u}_{h,k}^{(n)}} \delta \mathbf{u}_{h,k}^{(n)} \right) \cdot \tilde{\mathbf{u}}_h \\ & + \delta \lambda_{h,k}^{(n)} (\tilde{\mathbf{u}}_h \cdot \mathbf{n}_h) + \tilde{\lambda}_h \left( \delta \mathbf{u}_{h,k}^{(n)} \cdot \mathbf{n}_h \right) \, ds - \int_{\partial \Gamma_h \setminus l_{v,h}} \delta \mathbf{u}_{h,k}^{(n)} \cdot \mathbf{n}_{\tau,h} \tilde{p}_h \, dl \\ & = - \int_{\Gamma_h} \rho \frac{\theta_m \mathbf{u}_{h,k}^{(n)} - \mathbf{u}_{h,m}^{(n-1)}}{\Delta t} \cdot \tilde{\mathbf{u}}_h + \rho \left[ (\mathbf{u}_{h,k}^{(n)} \cdot \nabla_{\Gamma_h}) \mathbf{u}_{h,k}^{(n)} \right] \cdot \tilde{\mathbf{u}}_h \\ & + \frac{\mu}{2} \left( \nabla_{\Gamma_h} \mathbf{u}_{h,k}^{(n)} + \nabla_{\Gamma_h}^T \mathbf{u}_{h,k}^{(n)} \right) : \left( \nabla_{\Gamma_h} \tilde{\mathbf{u}}_h + \nabla_{\Gamma_h}^T \tilde{\mathbf{u}}_h \right) - p_{h,k}^{(n)} \operatorname{div}_{\Gamma_h} \tilde{\mathbf{u}}_h \\ & + \mathbf{u}_{h,k}^{(n)} \cdot \nabla_{\Gamma_h} \tilde{p}_h + \left( \alpha_h \mathbf{u}_{h,k}^{(n)} - \chi_h \mathbf{b}_{p,h}^{(n)} \left( \mathbf{u}_{h,k}^{(n)} \right) \right) \cdot \tilde{\mathbf{u}}_h + \lambda_{h,k}^{(n)} (\tilde{\mathbf{u}}_h \cdot \mathbf{n}_h) \\ & + \tilde{\lambda}_h \left( \mathbf{u}_{h,k}^{(n)} \cdot \mathbf{n}_h \right) \, ds + \int_{l_{v,h}} \mathbf{u}_{l_v} \cdot \mathbf{n}_{\tau,h} \tilde{p}_h \, dl + \int_{\partial \Gamma_h \setminus l_{v,h}} \mathbf{u}_{h,k}^{(n)} \cdot \mathbf{n}_{\tau,h} \tilde{p}_h \, dl \end{aligned} \quad (34)$$

By setting

$$\left\{ \begin{array}{l} R_{\mathbf{u}_t, k}^{(n)}(\tilde{\mathbf{u}}_h) := - \int_{\Gamma_h} \rho \frac{\theta_m \mathbf{u}_{h,k}^{(n)} - \mathbf{u}_{h,m}^{(n-1)}}{\Delta t} \cdot \tilde{\mathbf{u}}_h \, ds, \\ R_{\mathbf{u}, k}^{(n)}(\tilde{\mathbf{u}}_h) := - \int_{\Gamma_h} \rho \left[ \left( \mathbf{u}_{h,k}^{(n)} \cdot \nabla_{\Gamma_h} \right) \mathbf{u}_{h,k}^{(n)} \right] \cdot \tilde{\mathbf{u}}_h \\ \quad + \frac{\mu}{2} \left( \nabla_{\Gamma_h} \mathbf{u}_{h,k}^{(n)} + \nabla_{\Gamma_h}^T \mathbf{u}_{h,k}^{(n)} \right) : \left( \nabla_{\Gamma_h} \tilde{\mathbf{u}}_h + \nabla_{\Gamma_h}^T \tilde{\mathbf{u}}_h \right) \\ \quad - p_{h,k}^{(n)} \operatorname{div}_{\Gamma_h} \tilde{\mathbf{u}}_h + \left( \alpha_h \mathbf{u}_{h,k}^{(n)} - \chi_h \mathbf{b}_{p,h}^{(n)} \left( \mathbf{u}_{h,k}^{(n)} \right) \right) \cdot \tilde{\mathbf{u}}_h + \lambda_{h,k}^{(n)} (\tilde{\mathbf{u}}_h \cdot \mathbf{n}_h) \, ds, \\ R_{p,k}^{(n)}(\tilde{p}_h) := - \int_{\Gamma_h} \mathbf{u}_{h,k}^{(n)} \cdot \nabla_{\Gamma_h} \tilde{p}_h \, ds + \int_{l_{v,h}} \mathbf{u}_{l_v} \cdot \mathbf{n}_{\tau,h} \tilde{p}_h \, dl + \int_{\partial \Gamma_h \setminus l_{v,h}} \mathbf{u}_{h,k}^{(n)} \cdot \mathbf{n}_{\tau,h} \tilde{p}_h \, dl, \\ R_{\lambda,k}^{(n)}(\tilde{\lambda}_h) := - \int_{\Gamma_h} \tilde{\lambda}_h \left( \mathbf{u}_{h,k}^{(n)} \cdot \mathbf{n}_h \right) \, ds, \end{array} \right. \quad (35)$$

equation 34 can be equivalently transformed into

$$\left\{ \begin{array}{l} \int_{\Gamma_h} \rho \frac{\theta_m}{\Delta t} \delta \mathbf{u}_{h,k}^{(n)} \cdot \tilde{\mathbf{u}}_h + \rho \left[ \left( \mathbf{u}_{h,k}^{(n)} \cdot \nabla_{\Gamma_h} \right) \delta \mathbf{u}_{h,k}^{(n)} \right] \cdot \tilde{\mathbf{u}}_h + \rho \left[ \left( \delta \mathbf{u}_{h,k}^{(n)} \cdot \nabla_{\Gamma_h} \right) \mathbf{u}_{h,k}^{(n)} \right] \cdot \tilde{\mathbf{u}}_h \\ \quad + \frac{\mu}{2} \left( \nabla_{\Gamma_h} \delta \mathbf{u}_{h,k}^{(n)} + \nabla_{\Gamma_h}^T \delta \mathbf{u}_{h,k}^{(n)} \right) : \left( \nabla_{\Gamma_h} \tilde{\mathbf{u}}_h + \nabla_{\Gamma_h}^T \tilde{\mathbf{u}}_h \right) - \delta p_{h,k}^{(n)} \operatorname{div}_{\Gamma_h} \tilde{\mathbf{u}}_h \\ \quad + \left( \alpha_h \delta \mathbf{u}_{h,k}^{(n)} - \chi_h \frac{\partial \mathbf{b}_{p,h}^{(n)}}{\partial \mathbf{u}_{h,k}^{(n)}} \delta \mathbf{u}_{h,k}^{(n)} \right) \cdot \tilde{\mathbf{u}}_h + \delta \lambda_{h,k}^{(n)} (\tilde{\mathbf{u}}_h \cdot \mathbf{n}_h) \, ds = R_{\mathbf{u}_t, k}^{(n)}(\tilde{\mathbf{u}}_h) + R_{\mathbf{u}, k}^{(n)}(\tilde{\mathbf{u}}_h), \\ \int_{\Gamma_h} \delta \mathbf{u}_{h,k}^{(n)} \cdot \nabla_{\Gamma_h} \tilde{p}_h \, ds - \int_{\partial \Gamma_h \setminus l_{v,h}} \delta \mathbf{u}_{h,k}^{(n)} \cdot \mathbf{n}_{\tau,h} \tilde{p}_h \, dl = R_{p,k}^{(n)}(\tilde{p}_h), \\ \int_{\Gamma_h} \tilde{\lambda}_h \left( \delta \mathbf{u}_{h,k}^{(n)} \cdot \mathbf{n}_h \right) \, ds = R_{\lambda,k}^{(n)}(\tilde{\lambda}_h), \end{array} \right. \quad (36)$$

where  $R_{\mathbf{u}, k}^{(n)}(\tilde{\mathbf{u}}_h)$ ,  $R_{p,k}^{(n)}(\tilde{p}_h)$  and  $R_{\lambda,k}^{(n)}(\tilde{\lambda}_h)$  are the residuals associated with the variational formulation in equation 33.

Based on the nodal basis  $\{\psi_1^{(2)}, \psi_2^{(2)}, \dots, \psi_{N_2}^{(2)}\}$  for  $\mathcal{S}_h^{(2)}$ ,  $\mathbf{u}_{h,k}^{(n)}$ ,  $\delta \mathbf{u}_{h,k}^{(n)}$ ,  $\lambda_{h,k}^{(n)}$  and  $\delta \lambda_{h,k}^{(n)}$  have the following transformations:

$$\left\{ \begin{array}{l} \mathbf{u}_{h,k}^{(n)} = \sum_{i=1}^{N_2} \mathbf{U}_{k,i}^{(n)} \psi_i^{(2)}(\mathbf{x}) \\ \delta \mathbf{u}_{h,k}^{(n)} = \sum_{i=1}^{N_2} \Delta \mathbf{U}_{k,i}^{(n)} \psi_i^{(2)}(\mathbf{x}) \\ \lambda_{h,k}^{(n)} = \sum_{i=1}^{N_2} \Lambda_{k,i}^{(n)} \psi_i^{(2)}(\mathbf{x}) \\ \delta \lambda_{h,k}^{(n)} = \sum_{i=1}^{N_2} \Delta \Lambda_{k,i}^{(n)} \psi_i^{(2)}(\mathbf{x}) \end{array} \right\} \quad \text{at } \forall \mathbf{x} \in \Gamma_h, \quad (37)$$

where  $\mathbf{U}_{k,i}^{(n)}$ ,  $\Delta \mathbf{U}_{k,i}^{(n)}$ ,  $\Lambda_{k,i}^{(n)}$  and  $\Delta \Lambda_{k,i}^{(n)}$  are the nodal variables of  $\mathbf{u}_{h,k}^{(n)}$ ,  $\delta \mathbf{u}_{h,k}^{(n)}$ ,  $\lambda_{h,k}^{(n)}$  and  $\delta \lambda_{h,k}^{(n)}$ , respectively. Based on the nodal basis  $\{\psi_1^{(1)}, \psi_2^{(1)}, \dots, \psi_{N_1}^{(1)}\}$  for  $\mathcal{S}_h^{(1)}$ ,  $p_{h,k}^{(n)}$  and  $\delta p_{h,k}^{(n)}$  have the following transformations:

$$\left\{ \begin{array}{l} p_{h,k}^{(n)} = \sum_{i=1}^{N_1} P_{k,i}^{(n)} \psi_i^{(1)}(\mathbf{x}) \\ \delta p_{h,k}^{(n)} = \sum_{i=1}^{N_1} \Delta P_{k,i}^{(n)} \psi_i^{(1)}(\mathbf{x}) \end{array} \right\} \quad \text{at } \forall \mathbf{x} \in \Gamma_h, \quad (38)$$

where  $P_{k,i}^{(n)}$  and  $\Delta P_{k,i}^{(n)}$  are the nodal variables of  $p_{h,k}^{(n)}$  and  $\delta p_{h,k}^{(n)}$ , respectively. By substituting equation 37 and 38 into equation 36, and using the nodal basis of  $\mathcal{S}_h^{(2)}$  and  $\mathcal{S}_h^{(1)}$  as the test

functions, a linear system can be derived based on the assembly rule of stiffness matrix:

$$\begin{cases} [\mathbf{A} + \mathbf{B}_1 (\mathbf{U}_k^{(n)}) + \mathbf{B}_2 (\mathbf{U}_k^{(n)}) + \mathbf{C}] \Delta \mathbf{U}_k^{(n)} + \mathbf{D}_1 \Delta \mathbf{P}_k^{(n)} + \mathbf{E} (\boldsymbol{\Upsilon}_p) \Delta \mathbf{U}_k^{(n)} + \\ \mathbf{F} \Delta \boldsymbol{\Lambda}_k^{(n)} = \mathbf{R}_{\mathbf{u}_t, k}^{(n)} (\mathbf{U}_k^{(n)}, \mathbf{U}_k^{(n-1)}, \dots, \mathbf{U}_k^{(n-m)}) + \mathbf{R}_{\mathbf{u}, k}^{(n)} (\mathbf{U}_k^{(n)}, \mathbf{P}_k^{(n)}, \boldsymbol{\Lambda}_k^{(n)}; \boldsymbol{\Upsilon}_p), \\ \mathbf{D}_2^T \Delta \mathbf{U}_k^{(n)} = \mathbf{R}_{p, k}^{(n)} (\mathbf{U}_k^{(n)}), \\ \mathbf{F}^T \Delta \mathbf{U}_k^{(n)} = \mathbf{R}_{\lambda, k}^{(n)} (\mathbf{U}_k^{(n)}), \end{cases} \quad (39)$$

where  $\boldsymbol{\Upsilon}_p$  is a column vector corresponding to the discrete counterpart of the physical density  $\gamma_p$  in the current iteration of the topology optimization procedure in Table 1;  $\mathbf{R}_{\mathbf{u}_t, k}^{(n)}$  depends on  $\{\mathbf{U}_k^{(n-1)}, \mathbf{U}_k^{(n-2)}, \dots, \mathbf{U}_k^{(n-m)}\}$ , because  $\mathbf{u}_{h, m}^{(n-1)}$  is the linear combination of  $\{\mathbf{u}_h^{(n-1)}, \mathbf{u}_h^{(n-2)}, \dots, \mathbf{u}_h^{(n-m)}\}$ ;  $\mathbf{U}_k^{(n)}, \mathbf{P}_k^{(n)}, \boldsymbol{\Lambda}_k^{(n)}, \Delta \mathbf{U}_k^{(n)}, \Delta \mathbf{P}_k^{(n)}$  and  $\Delta \boldsymbol{\Lambda}_k^{(n)}$  are the discrete counterparts of  $\mathbf{u}_{h, k}^{(n)}, p_{h, k}^{(n)}, \lambda_{h, k}^{(n)}, \delta \mathbf{u}_{h, k}^{(n)}, \delta p_{h, k}^{(n)}$  and  $\delta \lambda_{h, k}^{(n)}$ , respectively; the discrete counterparts of  $\mathbf{u}_h^{(n)}, p_h^{(n)}$  and  $\lambda_h^{(n)}$  are

$$\begin{cases} \mathbf{U}^{(n)} := \mathbf{U}_k^{(n)} + \Delta \mathbf{U}_k^{(n)} \\ \mathbf{P}^{(n)} := \mathbf{P}_k^{(n)} + \Delta \mathbf{P}_k^{(n)} \\ \boldsymbol{\Lambda}^{(n)} := \boldsymbol{\Lambda}_k^{(n)} + \Delta \boldsymbol{\Lambda}_k^{(n)} \end{cases} \quad (40)$$

The correspondence between the matrixes in equation 39 and terms in equation 35 and 36 are provided in equation 61 and 62 of Appendix 7.2. The linear system in equation 39 can be rewritten into

$$\begin{pmatrix} \mathbf{A} + \mathbf{B}_1 + \mathbf{B}_2 + \mathbf{C} + \mathbf{E} & \mathbf{D}_1 & \mathbf{F} \\ \mathbf{D}_2^T & \mathbf{0} & \mathbf{0} \\ \mathbf{F}^T & \mathbf{0} & \mathbf{0} \end{pmatrix} \begin{pmatrix} \Delta \mathbf{U}_k^{(n)} \\ \Delta \mathbf{P}_k^{(n)} \\ \Delta \boldsymbol{\Lambda}_k^{(n)} \end{pmatrix} = \begin{pmatrix} \mathbf{R}_{\mathbf{u}_t, k}^{(n)} + \mathbf{R}_{\mathbf{u}, k}^{(n)} \\ \mathbf{R}_{p, k}^{(n)} \\ \mathbf{R}_{\lambda, k}^{(n)} \end{pmatrix}. \quad (41)$$

The boundary or interface condition of  $\mathbf{u}_h^{(n)}$  at  $l_{v, h}$  and point condition of  $p_h^{(n)}$  at  $\mathcal{P}_h$  can be imposed by using the elimination approach, with enforcing the linear system in equation 41 to be definite. The variational formulation in equation 10 can be solved by using the procedure in Table 2.

### 3.2.3 Discretization of variational formulation in equation 20

Based on the surface finite element method and  $m$ -step BDF schemes, the variational formulation (equation 20) for the adjoint surface Navier-Stokes equations is transformed into the formulation defined on  $\Gamma_h$  as:

for  $n' = N_t - 1, N_t - 2, \dots, 0$

$$\text{find } \begin{cases} \mathbf{u}_{a, h}^{(n')} \in (\mathcal{S}_h^{(2)})^3 \text{ with } \begin{cases} \mathbf{u}_{a, h}^{(n')} - (\mathbf{u}_{a, h}^{(n')} \cdot \mathbf{n}_{\tau, h}) \mathbf{n}_{\tau, h} = \mathbf{0} \text{ at } t = n' \Delta t, \forall \mathbf{x} \in l_{v, h} \\ \mathbf{u}_{a, h}^{(N_t)} = -\frac{1}{\rho} \frac{\partial C_h}{\partial \mathbf{u}_h^{(N_t)}} \text{ at } \forall \mathbf{x} \in \Gamma_h \end{cases} \\ p_{a, h}^{(n')} \in \mathcal{S}_h^{(1)} \text{ with } p_{a, h}^{(n')} (t, \mathbf{x}) = 0 \text{ at } t = n' \Delta t, \forall \mathbf{x} \in \mathcal{P}_h, \\ \lambda_{a, h}^{(n')} \in \mathcal{S}_h^{(2)} \text{ with } \lambda_{a, h}^{(n')} = 0 \text{ at } t = n' \Delta t, \forall \mathbf{x} \in l_{v, h}, \end{cases},$$

$$\begin{aligned} & \text{satisfying } \int_{\Gamma_h} \frac{\partial A_h^{(n')}}{\partial \mathbf{u}_h^{(n')}} \cdot \tilde{\mathbf{u}}_{a, h} + \frac{\partial A_h^{(n')}}{\partial \nabla_{\Gamma_h} \mathbf{u}_h^{(n')}} : \nabla_{\Gamma_h} \tilde{\mathbf{u}}_{a, h} + \frac{\partial A_h^{(n')}}{\partial p_h^{(n')}} \tilde{p}_{a, h} \\ & + \rho \frac{\theta_m \mathbf{u}_{a, h}^{(n')} - \mathbf{u}_{a, h, m}^{(n'+1)}}{\Delta t} \cdot \tilde{\mathbf{u}}_{a, h} + \rho \left[ (\tilde{\mathbf{u}}_{a, h} \cdot \nabla_{\Gamma_h}) \mathbf{u}_h^{(n')} + (\mathbf{u}_h^{(n')} \cdot \nabla_{\Gamma_h}) \tilde{\mathbf{u}}_{a, h} \right] \cdot \mathbf{u}_{a, h}^{(n')} \\ & + \frac{\mu}{2} \left( \nabla_{\Gamma_h} \mathbf{u}_{a, h}^{(n')} + \nabla_{\Gamma_h}^T \mathbf{u}_{a, h}^{(n')} \right) : \left( \nabla_{\Gamma_h} \tilde{\mathbf{u}}_{a, h} + \nabla_{\Gamma_h}^T \tilde{\mathbf{u}}_{a, h} \right) + \left( \alpha_h \mathbf{I} - \chi_h \frac{\partial \mathbf{b}_{p, h}^{(n')}}{\partial \mathbf{u}_h^{(n')}} \right) \mathbf{u}_{a, h}^{(n')} \cdot \tilde{\mathbf{u}}_{a, h} \\ & + \mathbf{u}_{a, h}^{(n')} \cdot \nabla_{\Gamma_h} \tilde{p}_{a, h} - p_{a, h}^{(n')} \text{div}_{\Gamma_h} \tilde{\mathbf{u}}_{a, h} + \left( \tilde{\lambda}_{a, h} \mathbf{u}_{a, h}^{(n')} + \lambda_{a, h}^{(n')} \tilde{\mathbf{u}}_{a, h} \right) \cdot \mathbf{n}_h \, ds \\ & - \int_{\partial \Gamma_h} \left( \mathbf{u}_{a, h}^{(n')} \cdot \mathbf{n}_{\tau, h} - \frac{\partial B_h^{(n')}}{\partial p_h^{(n')}} \right) \tilde{p}_{a, h} \, dl - \int_{\partial \Gamma_h \setminus l_{v, h}} \frac{\partial B_h^{(n')}}{\partial \mathbf{u}_h^{(n')}} \cdot \tilde{\mathbf{u}}_{a, h} \, dl = 0, \end{aligned}$$

for  $\forall \tilde{\mathbf{u}}_{a, h} \in (\mathcal{S}_h^{(2)})^3, \forall \tilde{p}_{a, h} \in \mathcal{S}_h^{(1)}$  and  $\tilde{\lambda}_{a, h} \in \mathcal{S}_h^{(2)}$

(42)

---

**Algorithm 2:** surface finite element solution of equation 10

---

Set  $\begin{cases} n \leftarrow 1 \\ k \leftarrow 1 \end{cases}$  and  $\begin{cases} \mathbf{U}_k^{(n-1)} \leftarrow \mathbf{u}_0 \\ \mathbf{U}_k^{(n)} \leftarrow \mathbf{0} \\ \mathbf{P}_k^{(n)} \leftarrow \mathbf{0} \\ \mathbf{\Lambda}_k^{(n)} \leftarrow \mathbf{0} \end{cases};$

**loop 1** (BDF)

**loop 2** (Newton iteration)

    Compute  $\{\mathbf{R}_{\mathbf{u}_t, k}^{(n)}, \mathbf{R}_{\mathbf{u}, k}^{(n)}, \mathbf{R}_{p, k}^{(n)}, \mathbf{R}_{\lambda, k}^{(n)}\}$  based on  $\{\mathbf{U}_k^{(n)}, \mathbf{U}_k^{(n-1)}, \mathbf{U}_k^{(n-2)}, \dots, \mathbf{U}_k^{(n-m)}, \mathbf{P}_k^{(n)}, \mathbf{\Lambda}_k^{(n)}\};$

    Assemble  $\{\mathbf{A}, \mathbf{B}_1, \mathbf{B}_2, \mathbf{C}, \mathbf{D}_1, \mathbf{D}_2, \mathbf{E}, \mathbf{F}\}$  based on  $\{\mathbf{U}_k^{(n)}, \mathbf{P}_k^{(n)}, \mathbf{\Lambda}_k^{(n)}\};$

    Solve the definite linear system corresponding to equation 41 by using a PARDISO solver;

    Compute  $\begin{cases} \mathbf{U}_{k+1}^{(n)} = \mathbf{U}_k^{(n)} + \Delta \mathbf{U}_k^{(n)} \\ \mathbf{P}_{k+1}^{(n)} = \mathbf{P}_k^{(n)} + \Delta \mathbf{P}_k^{(n)} \\ \mathbf{\Lambda}_{k+1}^{(n)} = \mathbf{\Lambda}_k^{(n)} + \Delta \mathbf{\Lambda}_k^{(n)} \end{cases};$

**if**  $\begin{cases} \frac{\|\Delta \mathbf{U}_k^{(n)}\|_2}{\|\mathbf{U}_k^{(n)}\|_2} \geq 10^{-6} \\ \frac{\|\Delta \mathbf{P}_k^{(n)}\|_2}{\|\mathbf{P}_k^{(n)}\|_2} \geq 10^{-6} \\ \frac{\|\Delta \mathbf{\Lambda}_k^{(n)}\|_2}{\|\mathbf{\Lambda}_k^{(n)}\|_2} \geq 10^{-6} \end{cases}$

$k \leftarrow k + 1;$

**else**

      Set  $\begin{cases} \mathbf{U}^{(n)} \leftarrow \mathbf{U}_{k+1}^{(n)} \\ \mathbf{P}^{(n)} \leftarrow \mathbf{P}_{k+1}^{(n)} \\ \mathbf{\Lambda}^{(n)} \leftarrow \mathbf{\Lambda}_{k+1}^{(n)} \end{cases},$  break **loop 2**, and continue **loop 1**;

**end if**

**end loop 2**

**if**  $n\Delta t < T$

$n \leftarrow n + 1;$

**else**

    break **loop 1**;

**end if**

**end loop 1**

---

Table 2: Pseudo codes used to solve the variational formulation in equation 10, where  $\mathbf{U}^{(n)}$ ,  $\mathbf{P}^{(n)}$  and  $\mathbf{\Lambda}^{(n)}$  are the discrete counterparts of  $\mathbf{u}_h^{(n)}$ ,  $p_h^{(n)}$  and  $\lambda_h^{(n)}$ , respectively;  $\|\cdot\|_2$  is the operator for 2-norm of a vector.

where  $n'$  is the time step number, and it is used as the superscript of the relevant variables and functions to denote the time step;  $\mathbf{u}_{a,h}^{(n')}$ ,  $p_{a,h}^{(n')}$  and  $\lambda_{a,h}^{(n')}$  are the adjoint variables of the fluidic velocity  $\mathbf{u}_h^{(n')}$ , pressure  $p_h^{(n')}$  and Lagrangian multiplier  $\lambda_h^{(n')}$  on  $\Gamma_h$  at time  $t = n'\Delta t$ , respectively;  $\tilde{\mathbf{u}}_{a,h}$ ,  $\tilde{p}_{a,h}$  and  $\tilde{\lambda}_{a,h}$  are the test functions of  $\mathbf{u}_{a,h}^{(n')}$ ,  $p_{a,h}^{(n')}$  and  $\lambda_{a,h}^{(n')}$ , respectively;  $A_h$ ,  $B_h$  and  $C_h$  are the integration functions of the optimization objective on  $\Gamma_h$ ; for the  $m$ -step BDF schemes, the expression of  $\mathbf{u}_{a,h,m}^{(n'+1)}$  is provided in Appendix 7.1 and it is determined by the linear combination of  $\{\mathbf{u}_{a,h}^{(n'+1)}, \mathbf{u}_{a,h}^{(n'+2)}, \dots, \mathbf{u}_{a,h}^{(n'+m)}\}$  with  $n' + m = N_t$ . By setting

$$\begin{cases} F_{\mathbf{u}_{at}}^{(n')}(\tilde{\mathbf{u}}_{a,h}) := \int_{\Gamma_h} \rho \frac{1}{\Delta t} \mathbf{u}_{a,h,m}^{(n'+1)} \cdot \tilde{\mathbf{u}}_{a,h} \, ds, \\ F_{\mathbf{u}_a}^{(n')}(\tilde{\mathbf{u}}_{a,h}) := - \int_{\Gamma_h} \frac{\partial A_h^{(n')}}{\partial \mathbf{u}_h^{(n')}} \cdot \tilde{\mathbf{u}}_{a,h} + \frac{\partial A_h^{(n')}}{\partial \nabla_{\Gamma_h} \mathbf{u}_h^{(n')}} : \nabla_{\Gamma_h} \tilde{\mathbf{u}}_{a,h} \, ds - \int_{\partial \Gamma_h \setminus l_{v,h}} \frac{\partial B_h^{(n')}}{\partial \mathbf{u}_h^{(n')}} \cdot \tilde{\mathbf{u}}_{a,h} \, dl, \\ F_{p_a}^{(n')}(\tilde{p}_{a,h}) := - \int_{\Gamma_h} \frac{\partial A_h^{(n')}}{\partial p_h^{(n')}} \tilde{p}_{a,h} \, ds + \int_{\partial \Gamma_h} \frac{\partial B_h^{(n')}}{\partial p_h^{(n')}} \tilde{p}_{a,h} \, dl, \end{cases} \quad (43)$$

equation 42 can be equivalently transformed into

$$\begin{cases} \int_{\Gamma_h} \rho \frac{\theta_m}{\Delta t} \mathbf{u}_{a,h}^{(n')} \cdot \tilde{\mathbf{u}}_{a,h} + \rho \left[ (\tilde{\mathbf{u}}_{a,h} \cdot \nabla_{\Gamma_h}) \mathbf{u}_h^{(n')} + (\mathbf{u}_h^{(n')} \cdot \nabla_{\Gamma_h}) \tilde{\mathbf{u}}_{a,h} \right] \cdot \mathbf{u}_{a,h}^{(n')} \\ + \frac{\mu}{2} \left( \nabla_{\Gamma_h} \mathbf{u}_{a,h}^{(n')} + \nabla_{\Gamma_h}^T \mathbf{u}_{a,h}^{(n')} \right) : \left( \nabla_{\Gamma_h} \tilde{\mathbf{u}}_{a,h} + \nabla_{\Gamma_h}^T \tilde{\mathbf{u}}_{a,h} \right) + \left( \alpha_h \mathbf{I} - \chi_h \frac{\partial \mathbf{b}_{p,h}^{(n')}}{\partial \mathbf{u}_h^{(n')}} \right) \mathbf{u}_{a,h}^{(n')} \cdot \tilde{\mathbf{u}}_{a,h} \\ - p_{a,h}^{(n')} \operatorname{div}_{\Gamma_h} \tilde{\mathbf{u}}_{a,h} + \lambda_{a,h}^{(n')} \tilde{\mathbf{u}}_{a,h} \cdot \mathbf{n}_h \, ds = F_{\mathbf{u}_{at}}^{(n')}(\tilde{\mathbf{u}}_{a,h}) + F_{\mathbf{u}_a}^{(n')}(\tilde{\mathbf{u}}_{a,h}), \\ \int_{\Gamma_h} \mathbf{u}_{a,h}^{(n')} \cdot \nabla_{\Gamma_h} \tilde{p}_{a,h} \, ds - \int_{\partial \Gamma_h} \mathbf{u}_{a,h}^{(n')} \cdot \mathbf{n}_{\tau,h} \tilde{p}_{a,h} \, dl = F_{p_a}^{(n')}(\tilde{p}_{a,h}), \\ \int_{\Gamma_h} \tilde{\lambda}_{a,h} \mathbf{u}_{a,h}^{(n')} \cdot \mathbf{n}_h \, ds = 0, \end{cases} \quad (44)$$

where  $F_{\mathbf{u}_a}^{(n')}(\tilde{\mathbf{u}}_{a,h})$  and  $F_{p_a}^{(n')}(\tilde{p}_{a,h})$  are the sources associated with the variational formulation in equation 42.

The discretized variational formulation for the adjoint surface Navier-Stokes equations (equation 42) can be solved directly, because it is linear. Based on the nodal basis  $\{\psi_1^{(2)}, \psi_2^{(2)}, \dots, \psi_{N_2}^{(2)}\}$  for  $\mathcal{S}_h^{(2)}$ ,  $\mathbf{u}_{a,h}^{(n')}$  and  $\lambda_{a,h}^{(n')}$  have the following transformations:

$$\left. \begin{aligned} \mathbf{u}_{a,h}^{(n')} &= \sum_{i=1}^{N_2} \mathbf{U}_{a,i}^{(n')} \psi_i^{(2)}(\mathbf{x}) \\ \lambda_{a,h}^{(n')} &= \sum_{i=1}^{N_2} \Lambda_{a,i}^{(n')} \psi_i^{(2)}(\mathbf{x}) \end{aligned} \right\} \text{ at } \forall \mathbf{x} \in \Gamma_h, \quad (45)$$

where  $\mathbf{U}_{a,i}^{(n')}$  and  $\Lambda_{a,i}^{(n')}$  are the nodal variables of  $\mathbf{u}_{a,h}^{(n')}$  and  $\lambda_{a,h}^{(n')}$ , respectively. Based on the nodal basis  $\{\psi_1^{(1)}, \psi_2^{(1)}, \dots, \psi_{N_1}^{(1)}\}$  for  $\mathcal{S}_h^{(1)}$ ,  $p_{a,h}^{(n')}$  has the following transformation:

$$p_{a,h}^{(n')} = \sum_{i=1}^{N_1} P_{a,i}^{(n')} \psi_i^{(1)}(\mathbf{x}), \text{ at } \forall \mathbf{x} \in \Gamma_h \quad (46)$$

where  $P_{a,i}^{(n')}$  is the nodal variable of  $p_{a,h}^{(n')}$ . By substituting equation 45 and 46 into equation 42, and using the nodal basis of  $\mathcal{S}_h^{(2)}$  and  $\mathcal{S}_h^{(1)}$  as the test functions, a linear system can be derived

based on the assembly rule of stiffness matrix:

$$\begin{cases} [\mathbf{A} + \mathbf{B}_1 (\mathbf{U}^{(n')}) + \mathbf{B}_2 (\mathbf{U}^{(n')}) + \mathbf{C}] \mathbf{U}_a^{(n')} + \mathbf{D}_1 \mathbf{P}_a^{(n')} + \mathbf{E} (\boldsymbol{\Upsilon}_p) \mathbf{U}_a^{(n')} + \\ \mathbf{F} \boldsymbol{\Lambda}_a^{(n')} = \mathbf{F}_{\mathbf{u}_{at}}^{(n')} (\mathbf{U}_a^{(n'+1)}, \mathbf{U}_a^{(n'+2)}, \dots, \mathbf{U}_a^{(n'+m)}) + \mathbf{F}_{\mathbf{u}_a}^{(n')} (\mathbf{U}^{(n')}, \mathbf{P}^{(n')}; \boldsymbol{\Upsilon}_p), \\ \mathbf{D}_2^T \mathbf{U}_a^{(n')} = \mathbf{F}_{p_a}^{(n')} (\mathbf{U}^{(n')}, \mathbf{P}^{(n')}; \boldsymbol{\Upsilon}_p), \\ \mathbf{F}^T \mathbf{U}_a^{(n')} = \mathbf{0}, \end{cases} \quad (47)$$

where  $\mathbf{F}_{\mathbf{u}_{at}}^{(n')}$  depends on  $\{\mathbf{U}_a^{(n'+1)}, \mathbf{U}_a^{(n'+2)}, \dots, \mathbf{U}_a^{(n'+m)}\}$ , because  $\mathbf{u}_{a,h,m}^{(n'+1)}$  is the linear combination of  $\{\mathbf{u}_{a,h}^{(n'+1)}, \mathbf{u}_{a,h}^{(n'+2)}, \dots, \mathbf{u}_{a,h}^{(n'+m)}\}$ ;  $\mathbf{U}_a^{(n')}$ ,  $\mathbf{P}_a^{(n')}$  and  $\boldsymbol{\Lambda}_a^{(n')}$  are the discrete counterparts of  $\mathbf{u}_{a,h}^{(n')}$ ,  $p_{a,h}^{(n')}$  and  $\lambda_{a,h}^{(n')}$ , respectively. The correspondence between the matrixes in equation 47 and terms in equation 43 and 44 are provided in equation 63 and 64 of Appendix 7.2. The linear system in equation 47 can be rewritten into

$$\begin{pmatrix} \mathbf{A} + \mathbf{B}_1 + \mathbf{B}_2 + \mathbf{C} + \mathbf{E} & \mathbf{D}_1 & \mathbf{F} \\ \mathbf{D}_2^T & \mathbf{0} & \mathbf{0} \\ \mathbf{F}^T & \mathbf{0} & \mathbf{0} \end{pmatrix} \begin{pmatrix} \mathbf{U}_a^{(n')} \\ \mathbf{P}_a^{(n')} \\ \boldsymbol{\Lambda}_a^{(n')} \end{pmatrix} = \begin{pmatrix} \mathbf{F}_{\mathbf{u}_{at}}^{(n')} + \mathbf{F}_{\mathbf{u}_a}^{(n')} \\ \mathbf{F}_{p_a}^{(n')} \\ \mathbf{0} \end{pmatrix}. \quad (48)$$

The boundary or interface condition of  $\mathbf{u}_{a,h}^{(n')}$  at  $l_{v,h}$  and point condition of  $p_{a,h}^{(n')}$  at  $\mathcal{P}_h$  can be imposed by using the elimination approach, to enforce the linear system in equation 48 to be definite. The variational formulation in equation 20 can be solved by using the procedure in Table 3.

---

**Algorithm 3:** surface finite element solution of equation 20

---

Solve  $\{\mathbf{U}^{(n)}, \mathbf{P}^{(n)}, \boldsymbol{\Lambda}^{(n)}\}$  ( $n = 1, 2, \dots, N_t$ ) by using Algorithm 2 in Table 2;

**for**  $n = 1, 2, \dots, N_t$

$n' = N_t - n$ ;

**loop** (BDF)

    Compute  $\{\mathbf{F}_{\mathbf{u}_{at}}, \mathbf{F}_{\mathbf{u}_a}, \mathbf{F}_{p_a}\}$  based on  $\{\mathbf{U}^{(n')}, \mathbf{P}^{(n')}, \boldsymbol{\Lambda}^{(n')}, \mathbf{U}_a^{(n'+1)}, \dots, \mathbf{U}_a^{(n'+m)}\}$ ;

    Assemble  $\{\mathbf{A}, \mathbf{B}_1, \mathbf{B}_2, \mathbf{C}, \mathbf{D}_1, \mathbf{D}_2, \mathbf{E}, \mathbf{F}\}$  based on  $\mathbf{U}^{(n')}$ ;

    Solve the definite linear system corresponding to equation 48 by using a PARDISO solver;

    Compute  $\{\mathbf{U}_a^{(n')}, \mathbf{P}_a^{(n')}, \boldsymbol{\Lambda}_a^{(n')}\}$ ;

**if**  $n' \Delta t > 0$

$n' \leftarrow n' - 1$ ;

**else**

        Break;

**end if**

**end loop** (BDF)

**end for**

---

Table 3: Pseudo codes used to solve the variational formulation in equation 20.

### 3.2.4 Discretization of variational formulation in equation 21

Based on the surface finite element method, the variational formulation (equation 21) for the adjoint equation of the surface-PDE filter is transformed into the following formulation defined on  $\Gamma_h$  as:

$$\begin{aligned} & \text{find } \gamma_{fa,h} \in \mathcal{S}_h^{(1)}, \text{ satisfying} \\ & \frac{1}{2T} \sum_{n=1}^{N_t} \int_{\Gamma_h} \left[ \frac{\partial (A_h^{(n-1)} + A_h^{(n)})}{\partial \gamma_{p,h}} + \frac{\partial \alpha_h}{\partial \gamma_{p,h}} (\mathbf{u}_h^{(n-1)} \cdot \mathbf{u}_{a,h}^{(n-1)} + \mathbf{u}_h^{(n)} \cdot \mathbf{u}_{a,h}^{(n)}) - \right. \\ & \left. \frac{\partial \chi_h}{\partial \gamma_{p,h}} (\mathbf{b}_{p,h}^{(n-1)} \cdot \mathbf{u}_{a,h}^{(n-1)} + \mathbf{b}_{p,h}^{(n)} \cdot \mathbf{u}_{a,h}^{(n)}) \right] \frac{\partial \gamma_{p,h}}{\partial \gamma_{f,h}} \tilde{\gamma}_{fa,h} \, ds + \int_{\Gamma_h} \frac{1}{T} \frac{\partial C_h}{\partial \gamma_{p,h}} \frac{\partial \gamma_{p,h}}{\partial \gamma_{f,h}} \tilde{\gamma}_{fa,h} \, ds \\ & + \int_{\Gamma_h} r_f^2 \nabla_{\Gamma_h} \gamma_{fa,h} \cdot \nabla_{\Gamma_h} \tilde{\gamma}_{fa,h} + \gamma_{fa,h} \tilde{\gamma}_{fa,h} \, ds = 0, \text{ for } \forall \tilde{\gamma}_{fa,h} \in \mathcal{S}_h^{(1)} \end{aligned} \quad (49)$$



where  $\gamma_{fa,h}$  is adjoint variable of the filtered design variable on  $\Gamma_h$ ; the time integration is implemented by using the trapezoid method.

Based on the nodal basis  $\{\psi_1^{(1)}, \psi_2^{(1)}, \dots, \psi_{N_1}^{(1)}\}$  for  $\mathcal{S}_h^{(1)}$ ,  $\gamma_{fa,h}$  has the following transformation:

$$\gamma_{fa,h} = \sum_{i=1}^{N_1} \Upsilon_{fa,h,i} \psi_i^{(1)}(\mathbf{x}), \text{ at } \forall \mathbf{x} \in \Gamma_h \quad (50)$$

where  $\Upsilon_{fa,h,i}$  is the nodal variable of  $\gamma_{fa,h}$ . By substituting equation 50 into equation 49, and using the nodal basis of  $\mathcal{S}_h^{(1)}$  as the test functions, a linear system can be derived based on the assembly rule of stiffness matrix:

$$(\mathbf{K} + \mathbf{N}) \Upsilon_{fa} = \mathbf{F}_{\gamma_{fa}} \left( \mathbf{U}^{(1)}, \dots, \mathbf{U}^{(N_t)}, \mathbf{P}^{(1)}, \dots, \mathbf{P}^{(N_t)}, \mathbf{U}_a^{(1)}, \dots, \mathbf{U}_a^{(N_t)}; \Upsilon_f \right), \quad (51)$$

where  $\Upsilon_{fa}$  is the discrete counterpart of  $\gamma_{fa,h}$ . The correspondence between the matrixes in equation 51 and terms in equation 49 are provided in Appendix 7.2. The variational formulation in equation 32 can be solved by using a PARDISO solver [86].

### 3.2.5 Computation of adjoint sensitivity in equation 19

Based on the finite element space in equation 28 and adjoint sensitivity in equation 19, the adjoint sensitivity of  $J$  on  $\Gamma_h$  is expressed as:

$$\Delta J_h = -T \int_{\Gamma_h} \gamma_{fa,h} \delta \gamma_h \, ds, \quad (52)$$

where  $\delta \gamma_h \in \mathcal{S}_h^{(1)}$  is the first order variational of  $\gamma_h$ . Based on equation 31,  $\delta \gamma_h$  is expressed as

$$\delta \gamma_h = \sum_{i=1}^{N_1} \Delta \Upsilon_{h,i} \psi_i^{(1)}(\mathbf{x}). \quad (53)$$

By substituting equation 50 and 53 into equation 52, the discretized adjoint sensitivity in equation 52 can be transformed into

$$\frac{\Delta J_h}{\Delta \Upsilon} = -T \mathbf{N} \Upsilon_{fa}, \quad (54)$$

where  $\Delta \Upsilon$  is the discrete counterpart of  $\delta \gamma_h$ .

### 3.2.6 Computation of adjoint sensitivity in equation 22

Based on the finite element space in equation 28 and adjoint sensitivity in equation 22, the adjoint sensitivity of  $v$  on  $\Gamma_h$  is expressed as:

$$\Delta v_h = -\frac{1}{|\Gamma_h|} \int_{\Gamma_h} \gamma_{fa,h} \delta \gamma_h \, ds. \quad (55)$$

By substituting equation 50 and 53 into equation 55, the discretized adjoint sensitivity in equation 55 can be transformed into

$$\frac{\Delta v_h}{\Delta \Upsilon} = -\frac{\mathbf{N} \Upsilon_{fa}}{\mathbf{1}^T \mathbf{N} \mathbf{1}}, \quad (56)$$

where  $\mathbf{1}$  is the  $N_1 \times 1$  column vector with 1 as its elements;  $|\Gamma_h|$  is computed as  $\mathbf{1}^T \mathbf{N} \mathbf{1}$ .

## 3.3 Notifications

- For steady cases: degenerate into the formulations of topology optimization for steady flows on 2-manifolds.
- For the matrixes in the linear systems: reuse the numerical information to effectively reduce the CPU-time cost.

## 4 Results and discussion

Topology optimization of surface flows is implemented on orientable and non-orientable 2-manifolds in this section.

## 4.1 Velocity-driven surface flows

In this section, the 2-manifolds corresponding to continuously deforming quadrangular planes into the shapes of a sphere, a torus and a Möbius strip are considered in this section. These 2-manifolds have been sketched in Figure 4, where the inlet boundaries with known velocity distributions, the no-slip boundaries and the open boundaries have been marked in different colors. The known velocity distributions are the parabolic functions of the arc-length coordinate of the inlet boundaries. These known velocity distributions satisfy the tangential constraint of the fluid velocity in equation 4.

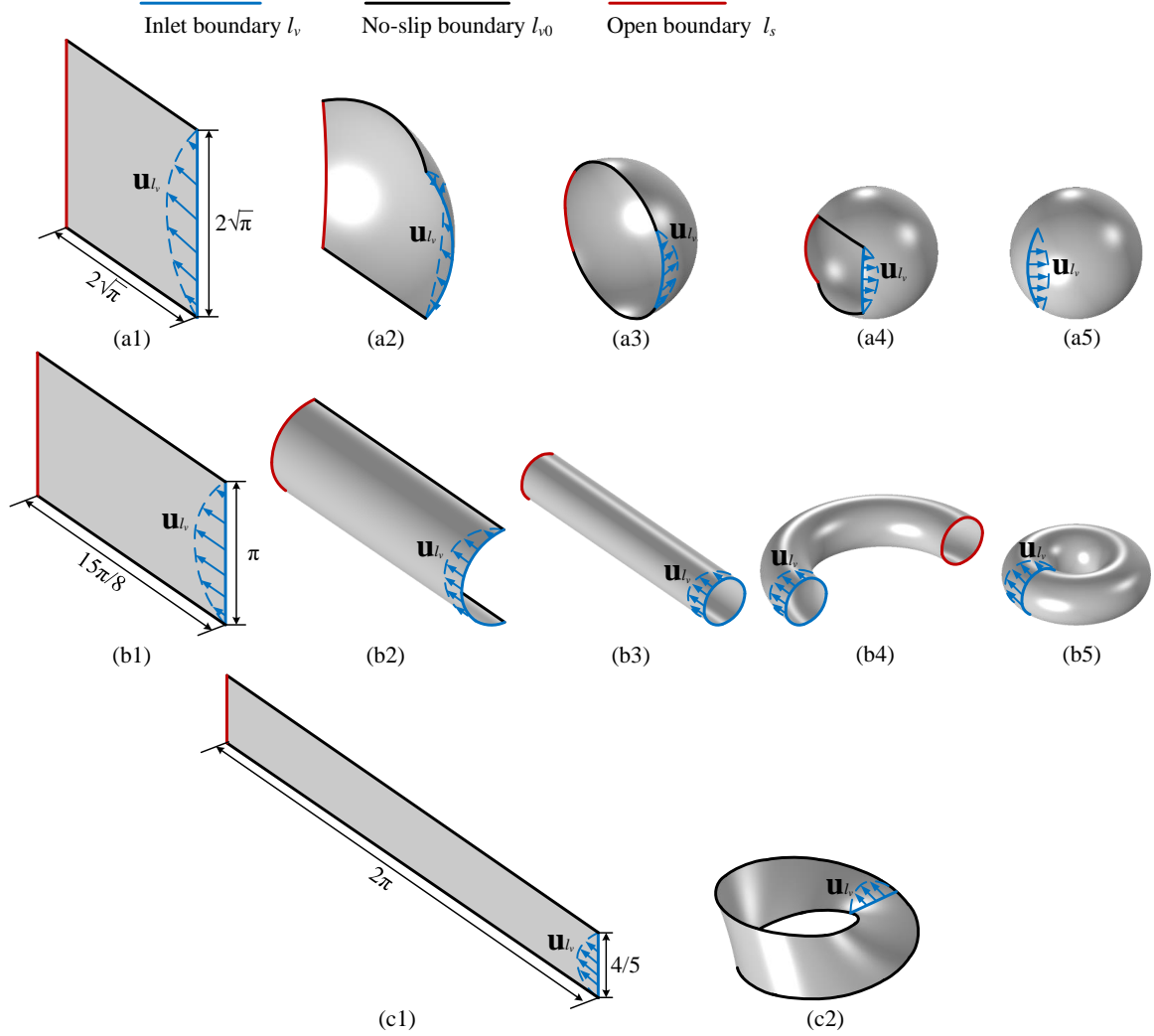


Figure 4: (a1-a5) 2-manifolds corresponding to continuously deforming a square plane into the shape of a sphere, where the areas of the 2-manifolds are kept to be constant. (b1-b5) 2-manifolds corresponding to continuously deforming a rectangular plane into the shape of a torus, where the areas of the 2-manifolds are kept to be constant. (c1-c2) 2-manifolds corresponding to deforming a rectangular strip into the shape of a Möbius strip, where the areas of the rectangular and Möbius strips are kept to be the same. The inlet boundaries with known velocity distributions, no-slip boundaries and open boundaries have been marked in blue, black and red colors, respectively.  $\mathbf{u}_{l_v}$ , satisfying the tangential constraint of the fluid velocity in equation 4, is a known velocity distribution which is a parabolic function of the arc-length coordinate of an inlet boundary.

## 4.2 Area force-driven surface flows

Centrifugal, Coriolis and Euler forces will be considered here. Those forces are generated by rotating 2-manifolds along some specified axes.

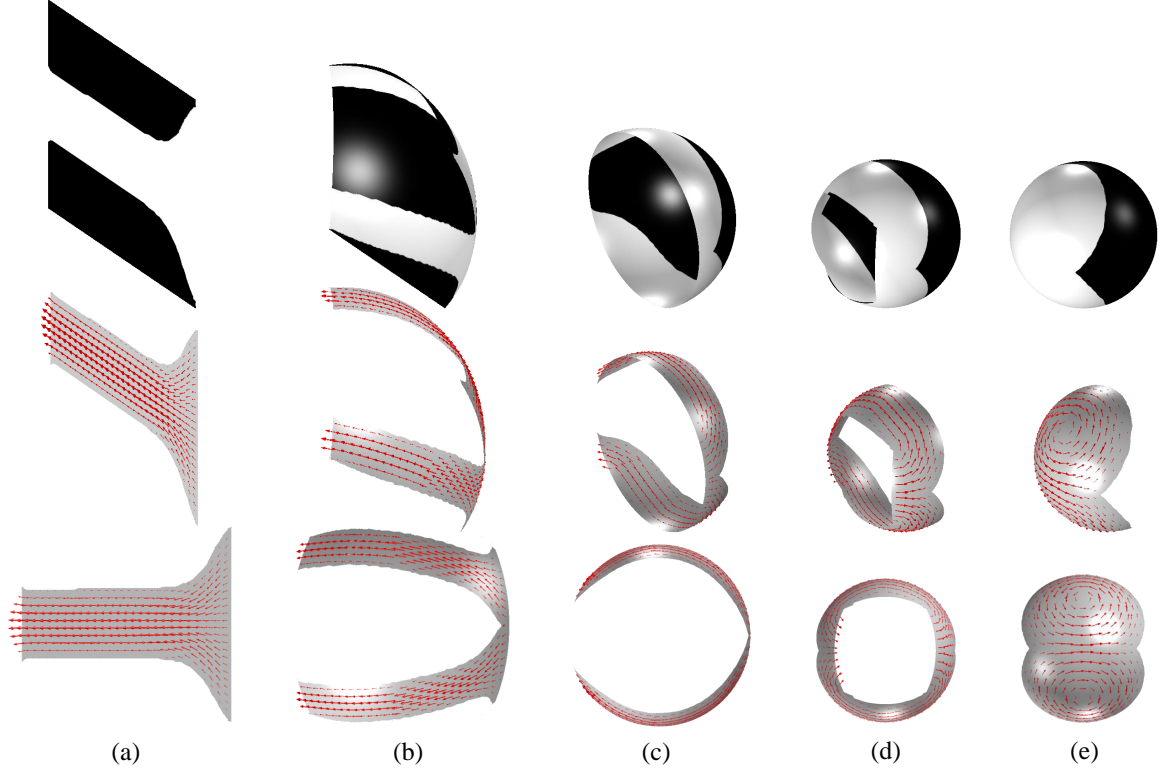


Figure 5: Topology optimization of steady surface flows on the 2-manifolds sketched in Figure 4(a1-a5) corresponding to continuously deforming a square plane into the shape of a sphere, where the design objective is to minimize the viscous dissipation of the surface flows driven by the inlet/interfacial velocity  $\mathbf{u}_{l_v}$  with  $\sup_{\mathbf{x} \in l_v} |\mathbf{u}_{l_v}| = 1$ . In the first row, the distributions of the material density are shown; in the second row, the patterns of the surface flows are shown; in the third row, the front views of the patterns of the surface flows are shown. In the second and third rows, the distributions of the velocity vectors are presented by the arrows marked in red color.

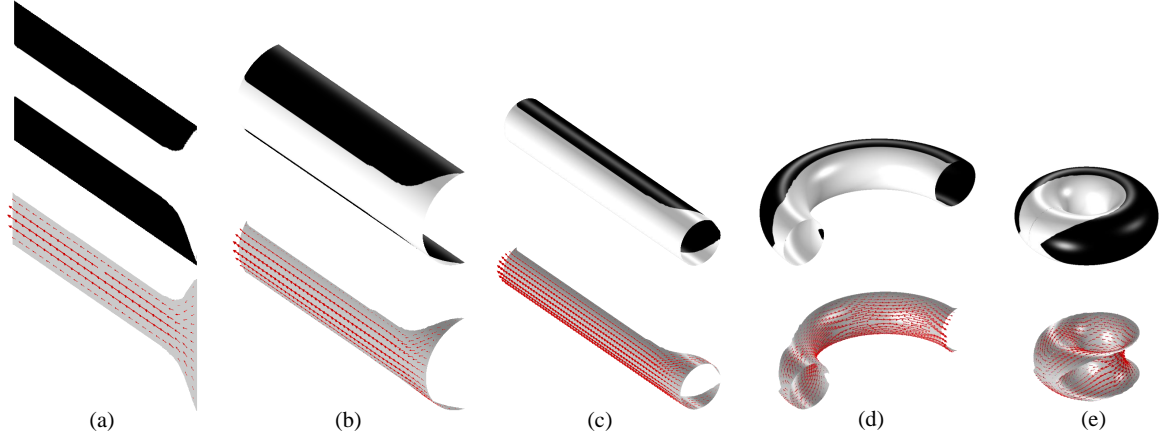


Figure 6: Topology optimization of steady surface flows on the 2-manifolds sketched in Figure 4(b1-b5) corresponding to continuously deforming a rectangular plane into the shape of a torus, where the design objective is to minimize the viscous dissipation of the surface flows driven by the inlet/interfacial velocity  $\mathbf{u}_{l_v}$  with  $\sup_{\mathbf{x} \in l_v} |\mathbf{u}_{l_v}| = 1$ . In the first row, the distributions of the material density are shown; in the second row, the patterns of the surface flows are shown, where the distributions of the velocity vectors are presented by the arrows marked in red color.

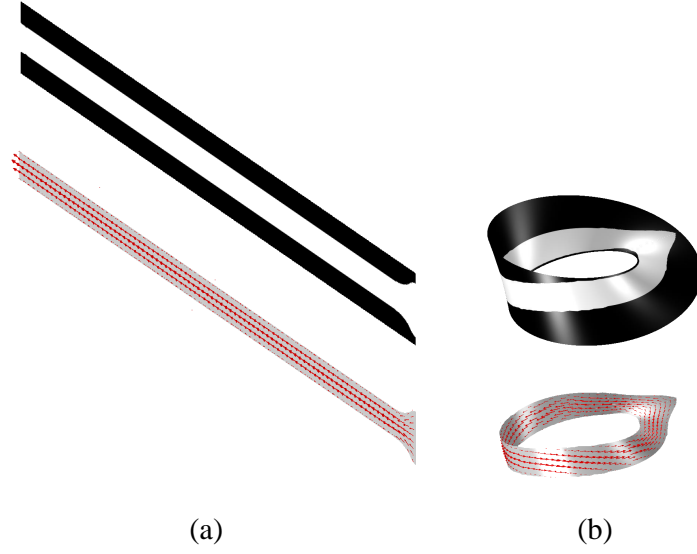


Figure 7: Topology optimization of steady surface flows on the 2-manifolds sketched in Figure 4(c1-c2) corresponding to deforming a rectangular strip into the shape of a Möbius strip, where the design objective is to minimize the viscous dissipation of the surface flows driven by the inlet/interfacial velocity  $\mathbf{u}_{l_v}$  with  $\sup_{\mathbf{x} \in l_v} |\mathbf{u}_{l_v}| = 1$ . In the first row, the distributions of the material density are shown; in the second row, the patterns of the surface flows are shown, where the distributions of the velocity vectors are presented by the arrows marked in red color.

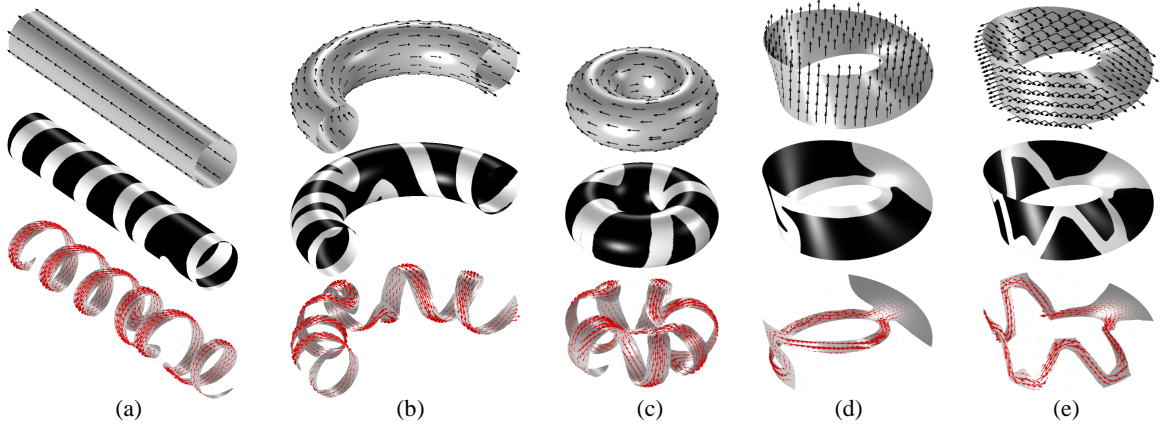


Figure 8: Topology optimization of steady surface flows on the 2-manifolds sketched in Figure 4(b3-b5 and c2), where the surface flows are driven by the inlet/interfacial velocity  $\mathbf{u}_{l_v}$  with  $\sup_{\mathbf{x} \in l_v} |\mathbf{u}_{l_v}| = 1$ . The design objective is to maximize the projected velocity distribution perpendicular to the vector distributions shown in the first row of this figure. In the second row, the distributions of the material density are shown; in the third row, the patterns of the surface flows are shown, where the distributions of the velocity vectors are presented by the arrows marked in red color.

### 4.3 Extension to convection-diffusion problems

Stabilization will be included in this section for the  $P1$ - $P1$  surface elements. Problems for mixing two fluids with different concentration of species will be used to demonstrate this extension.

## 5 Conclusions

Conclusions will be made in the near future.

## 6 Acknowledgements

Y. Deng acknowledges the support from a Humboldt Research Fellowship for Experienced Researchers (Humboldt-ID: 1197305), the National Natural Science Foundation of China (No. 51875545), and the Youth Innovation Promotion Association of the Chinese Academy of Sciences (No. 2018253); J.G. Korvink acknowledges support from an EU2020 FET grant (TiSuMR, 737043), the DFG under grant KO 1883/20-1 Metacoils, funding within the framework of the German Excellence Initiative under grant EXC 2082 "3D Matter Made to Order", and from the VirtMat initiative "Virtual Materials Design".

## 7 Appendix

This section provides the related parameters and expressions in the  $m$ -step BDF schemes, and the correspondence between the finite element matrixes and the terms of variational formulations.

### 7.1 Parameters and expressions in $m$ -step BDF schemes

In order to use the  $m$ -step BDF schemes to discretize the variational formulations of the surface Navier-Stokes equations and their adjoint equations, the values of the parameter  $\theta_m$  and expressions of  $\mathbf{u}_{h,m}^{(n-1)}$  and  $\mathbf{u}_{a,h,m}^{(n'+1)}$  are provided as follows.

The values of the parameter  $\theta_m$  are

$$\theta_m = \begin{cases} 1, & \text{for } m = 1 \\ \frac{3}{2}, & \text{for } m = 2 \\ \frac{11}{6}, & \text{for } m = 3 \\ \frac{25}{12}, & \text{for } m = 4 \\ \frac{137}{60}, & \text{for } m = 5 \\ \frac{147}{60}, & \text{for } m = 6 \end{cases}. \quad (57)$$

$\mathbf{u}_{h,m}^{(n-1)}$  is expressed based on the linear combination of  $\{\mathbf{u}_h^{(n-1)}, \mathbf{u}_h^{(n-2)}, \dots, \mathbf{u}_h^{(n-m)}\}$ :

$$\mathbf{u}_{h,m}^{(n-1)} = \begin{cases} \mathbf{u}_h^{(n-1)}, & \text{if } n \geq 1, \text{ for } m = 1 \\ 2\mathbf{u}_h^{(n-1)} - \frac{1}{2}\mathbf{u}_h^{(n-2)}, & \text{if } n \geq 2, \text{ for } m \leq 2 \\ 3\mathbf{u}_h^{(n-1)} - \frac{3}{2}\mathbf{u}_h^{(n-2)} + \frac{1}{3}\mathbf{u}_h^{(n-3)}, & \text{if } n \geq 3, \text{ for } m \leq 3 \\ 4\mathbf{u}_h^{(n-1)} - 3\mathbf{u}_h^{(n-2)} + \frac{4}{3}\mathbf{u}_h^{(n-3)} - \frac{1}{4}\mathbf{u}_h^{(n-4)}, & \text{if } n \geq 4, \text{ for } m \leq 4 \\ 5\mathbf{u}_h^{(n-1)} - 5\mathbf{u}_h^{(n-2)} + \frac{10}{3}\mathbf{u}_h^{(n-3)} - \frac{5}{4}\mathbf{u}_h^{(n-4)} + \frac{1}{5}\mathbf{u}_h^{(n-5)}, & \text{if } n \geq 5, \text{ for } m \leq 5 \\ 6\mathbf{u}_h^{(n-1)} - \frac{15}{2}\mathbf{u}_h^{(n-2)} + \frac{20}{3}\mathbf{u}_h^{(n-3)} - \frac{15}{4}\mathbf{u}_h^{(n-4)} + \frac{6}{5}\mathbf{u}_h^{(n-5)} - \frac{1}{6}\mathbf{u}_h^{(n-6)}, & \text{if } n \geq 6, \text{ for } m \leq 6 \end{cases}, \quad (58)$$

where  $\mathbf{u}_h^{(n-1)}$  is the initial distribution of the fluidic velocity  $\mathbf{u}_0$  for  $n = 1$ .  $\mathbf{u}_{a,h,m}^{(n'+1)}$  is expressed

based on the linear combination of  $\left\{ \mathbf{u}_{a,h}^{(n'+1)}, \mathbf{u}_{a,h}^{(n'+2)}, \dots, \mathbf{u}_{a,h}^{(n'+m)} \right\}$ :

$$\mathbf{u}_{a,h,m}^{(n'+1)} = \begin{cases} \mathbf{u}_{a,h}^{(n'+1)}, & \text{if } n \geq 1, \text{ for } m = 1 \\ 2\mathbf{u}_{a,h}^{(n'+1)} - \frac{1}{2}\mathbf{u}_{a,h}^{(n'+2)}, & \text{if } n \geq 2, \text{ for } m \leq 2 \\ 3\mathbf{u}_{a,h}^{(n'+1)} - \frac{3}{2}\mathbf{u}_{a,h}^{(n'+2)} + \frac{1}{3}\mathbf{u}_{a,h}^{(n'+3)}, & \text{if } n \geq 3, \text{ for } m \leq 3 \\ 4\mathbf{u}_{a,h}^{(n'+1)} - 3\mathbf{u}_{a,h}^{(n'+2)} + \frac{4}{3}\mathbf{u}_{a,h}^{(n'+3)} - \frac{1}{4}\mathbf{u}_{a,h}^{(n'+4)}, & \text{if } n \geq 4, \text{ for } m \leq 4 \\ 5\mathbf{u}_{a,h}^{(n'+1)} - 5\mathbf{u}_{a,h}^{(n'+2)} + \frac{10}{3}\mathbf{u}_{a,h}^{(n'+3)} - \frac{5}{4}\mathbf{u}_{a,h}^{(n'+4)} + \frac{1}{5}\mathbf{u}_{a,h}^{(n'+5)}, & \text{if } n \geq 5, \text{ for } m \leq 5 \\ 6\mathbf{u}_{a,h}^{(n'+1)} - \frac{15}{2}\mathbf{u}_{a,h}^{(n'+2)} + \frac{20}{3}\mathbf{u}_{a,h}^{(n'+3)} - \frac{15}{4}\mathbf{u}_{a,h}^{(n'+4)} + \frac{6}{5}\mathbf{u}_{a,h}^{(n'+5)} - \frac{1}{6}\mathbf{u}_{a,h}^{(n'+6)}, & \text{if } n \geq 6, \text{ for } m \leq 6 \end{cases}, \quad (59)$$

where  $\mathbf{u}_{a,h}^{(n'+1)}$  is the initial distribution of the adjoint fluidic velocity for  $n' = N_t - 1$ .

## 7.2 Correspondence between finite element matrixes and terms of variational formulations

For Section 3.2, the correspondence between the finite element matrixes of the linear systems and the terms of the variational formulations defined on the discretized 2-manifold are provided as follows.

The correspondence between the matrixes in equation 32 and the terms in equation 31 are described as:

$$\begin{cases} \mathbf{K}\Upsilon_f \longleftrightarrow \int_{\Gamma_h} r_f^2 \nabla_{\Gamma_h} \gamma_{f,h} \cdot \nabla_{\Gamma_h} \tilde{\gamma}_{f,h} \, ds, \\ \mathbf{N}\Upsilon_f \longleftrightarrow \int_{\Gamma_h} \gamma_{f,h} \tilde{\gamma}_{f,h} \, ds, \\ \mathbf{N}\Upsilon \longleftrightarrow \int_{\Gamma_h} \gamma_h \tilde{\gamma}_{f,h} \, ds. \end{cases} \quad (60)$$

The correspondence between the matrixes in equation 39 and the terms in equation 35 and 36 are described as:

$$\begin{cases} \mathbf{R}_{\mathbf{u}_t,k}^{(n)} \left( \mathbf{U}_k^{(n)}, \mathbf{U}_k^{(n-1)}, \dots, \mathbf{U}_k^{(n-m)} \right) \longleftrightarrow R_{\mathbf{u}_t,k}^{(n)} (\tilde{\mathbf{u}}_h), \\ \mathbf{R}_{\mathbf{u},k}^{(n)} \left( \mathbf{U}_k^{(n)}, \mathbf{P}_k^{(n)}, \mathbf{\Lambda}_k^{(n)}; \Upsilon_p \right) \longleftrightarrow R_{\mathbf{u},k}^{(n)} (\tilde{\mathbf{u}}_h), \\ \mathbf{R}_{p,k}^{(n)} \left( \mathbf{U}_k^{(n)} \right) \longleftrightarrow R_{p,k}^{(n)} (\tilde{p}_h), \\ \mathbf{R}_{\lambda,k}^{(n)} \left( \mathbf{U}_k^{(n)} \right) \longleftrightarrow R_{\lambda,k}^{(n)} (\tilde{\lambda}_h), \end{cases} \quad (61)$$

and

$$\left\{ \begin{array}{l} \mathbf{A} \Delta \mathbf{U}_k^{(n)} \longleftrightarrow \int_{\Gamma_h} \rho \frac{\theta_m}{\Delta t} \delta \mathbf{u}_{h,k}^{(n)} \cdot \tilde{\mathbf{u}}_h \, ds, \\ \mathbf{B}_1 \left( \mathbf{U}_k^{(n)} \right) \Delta \mathbf{U}_k^{(n)} \longleftrightarrow \int_{\Gamma_h} \rho \left[ \left( \mathbf{u}_{h,k}^{(n)} \cdot \nabla_{\Gamma_h} \right) \delta \mathbf{u}_{h,k}^{(n)} \right] \cdot \tilde{\mathbf{u}}_h \, ds, \\ \mathbf{B}_2 \left( \mathbf{U}_k^{(n)} \right) \Delta \mathbf{U}_k^{(n)} \longleftrightarrow \int_{\Gamma_h} \rho \left[ \left( \delta \mathbf{u}_{h,k}^{(n)} \cdot \nabla_{\Gamma_h} \right) \mathbf{u}_{h,k}^{(n)} \right] \cdot \tilde{\mathbf{u}}_h \, ds, \\ \mathbf{C} \Delta \mathbf{U}_k^{(n)} \longleftrightarrow \int_{\Gamma_h} \frac{\mu}{2} \left( \nabla_{\Gamma_h} \delta \mathbf{u}_{h,k}^{(n)} + \nabla_{\Gamma_h}^T \delta \mathbf{u}_{h,k}^{(n)} \right) : \left( \nabla_{\Gamma_h} \tilde{\mathbf{u}}_h + \nabla_{\Gamma_h}^T \tilde{\mathbf{u}}_h \right) \, ds, \\ \mathbf{D}_1 \Delta \mathbf{P}_k^{(n)} \longleftrightarrow \int_{\Gamma_h} -\delta p_{h,k}^{(n)} \operatorname{div}_{\Gamma_h} \tilde{\mathbf{u}}_h \, ds, \\ \mathbf{E} \left( \Upsilon_p \right) \Delta \mathbf{U}_k^{(n)} \longleftrightarrow \int_{\Gamma_h} \left( \alpha_h \delta \mathbf{u}_{h,k}^{(n)} - \chi_h \frac{\partial \mathbf{b}_{p,h}^{(n)}}{\partial \mathbf{u}_{h,k}^{(n)}} \delta \mathbf{u}_{h,k}^{(n)} \right) \cdot \tilde{\mathbf{u}}_h \, ds, \\ \mathbf{F} \Delta \Lambda_k^{(n)} \longleftrightarrow \int_{\Gamma_h} \delta \lambda_{h,k}^{(n)} (\tilde{\mathbf{u}}_h \cdot \mathbf{n}_h) \, ds, \\ \mathbf{D}_2^T \Delta \mathbf{U}_k^{(n)} \longleftrightarrow \int_{\Gamma_h} \delta \mathbf{u}_{h,k}^{(n)} \cdot \nabla_{\Gamma_h} \tilde{p}_h \, ds - \int_{\partial \Gamma_h \setminus l_{v,h}} \delta \mathbf{u}_{h,k}^{(n)} \cdot \mathbf{n}_{\tau,h} \tilde{p}_h \, dl, \\ \mathbf{F}^T \Delta \mathbf{U}_k^{(n)} \longleftrightarrow \int_{\Gamma_h} \tilde{\lambda}_h \left( \delta \mathbf{u}_{h,k}^{(n)} \cdot \mathbf{n}_h \right) \, ds. \end{array} \right. \quad (62)$$

The correspondence between the matrixes in equation 47 and the terms in equation 43 and 44 are described as:

$$\left\{ \begin{array}{l} \mathbf{F}_{\mathbf{u}_{at}}^{(n')} \left( \mathbf{U}_a^{(n'+1)}, \mathbf{U}_a^{(n'+2)}, \dots, \mathbf{U}_a^{(n'+m)} \right) \longleftrightarrow F_{\mathbf{u}_{at}}^{(n')} (\tilde{\mathbf{u}}_{a,h}), \\ \mathbf{F}_{\mathbf{u}_a}^{(n')} \left( \mathbf{U}^{(n')}, \mathbf{P}^{(n')}; \Upsilon_p \right) \longleftrightarrow F_{\mathbf{u}_a}^{(n')} (\tilde{\mathbf{u}}_{a,h}), \\ \mathbf{F}_{p_a}^{(n')} \left( \mathbf{U}^{(n')}, \mathbf{P}^{(n')}; \Upsilon_p \right) \longleftrightarrow F_{p_a}^{(n')} (\tilde{p}_{a,h}), \end{array} \right. \quad (63)$$

and

$$\left\{ \begin{array}{l} \mathbf{A} \mathbf{U}_a^{(n')} \longleftrightarrow \int_{\Gamma_h} \rho \frac{\theta_m}{\Delta t} \mathbf{u}_{a,h}^{(n')} \cdot \tilde{\mathbf{u}}_{a,h} \, ds, \\ \mathbf{B}_1 \left( \mathbf{U}^{(n')} \right) \mathbf{U}_a^{(n')} \longleftrightarrow \int_{\Gamma_h} \rho \left[ \left( \mathbf{u}_h^{(n')} \cdot \nabla_{\Gamma_h} \right) \tilde{\mathbf{u}}_{a,h} \right] \cdot \mathbf{u}_{a,h}^{(n')} \, ds, \\ \mathbf{B}_2 \left( \mathbf{U}^{(n')} \right) \mathbf{U}_a^{(n')} \longleftrightarrow \int_{\Gamma_h} \rho \left[ \left( \tilde{\mathbf{u}}_{a,h} \cdot \nabla_{\Gamma_h} \right) \mathbf{u}_h^{(n')} \right] \cdot \mathbf{u}_{a,h}^{(n')} \, ds, \\ \mathbf{C} \mathbf{U}_a^{(n')} \longleftrightarrow \int_{\Gamma_h} \frac{\mu}{2} \left( \nabla_{\Gamma_h} \mathbf{u}_{a,h}^{(n')} + \nabla_{\Gamma_h}^T \mathbf{u}_{a,h}^{(n')} \right) : \left( \nabla_{\Gamma_h} \tilde{\mathbf{u}}_{a,h} + \nabla_{\Gamma_h}^T \tilde{\mathbf{u}}_{a,h} \right) \, ds, \\ \mathbf{D}_1 \mathbf{P}_a^{(n')} \longleftrightarrow \int_{\Gamma_h} -p_{a,h}^{(n')} \operatorname{div}_{\Gamma_h} \tilde{\mathbf{u}}_{a,h} \, ds, \\ \mathbf{E} \left( \Upsilon_p \right) \mathbf{U}_a^{(n')} \longleftrightarrow \int_{\Gamma_h} \left( \alpha_h \mathbf{I} - \chi_h \frac{\partial \mathbf{b}_{p,h}^{(n')}}{\partial \mathbf{u}_h^{(n')}} \right) \mathbf{u}_{a,h}^{(n')} \cdot \tilde{\mathbf{u}}_{a,h} \, ds, \\ \mathbf{F} \Lambda_a^{(n')} \longleftrightarrow \int_{\Gamma_h} \lambda_{a,h}^{(n')} \tilde{\mathbf{u}}_{a,h} \cdot \mathbf{n}_h \, ds, \\ \mathbf{D}_2^T \mathbf{U}_a^{(n')} \longleftrightarrow \int_{\Gamma_h} \mathbf{u}_{a,h}^{(n')} \cdot \nabla_{\Gamma_h} \tilde{p}_{a,h} \, ds - \int_{\partial \Gamma_h} \mathbf{u}_{a,h}^{(n')} \cdot \mathbf{n}_{\tau,h} \tilde{p}_{a,h} \, dl, \\ \mathbf{F}^T \mathbf{U}_a^{(n')} \longleftrightarrow \int_{\Gamma_h} \tilde{\lambda}_{a,h} \mathbf{u}_{a,h}^{(n')} \cdot \mathbf{n}_h \, ds. \end{array} \right. \quad (64)$$

The correspondence between the matrixes in equation 51 and the terms in equation 49 are

described as:

$$\left\{ \begin{array}{l} \mathbf{K}\Upsilon_f \longleftrightarrow \int_{\Gamma_h} r_f^2 \nabla_{\Gamma_h} \gamma_{fa,h} \cdot \nabla_{\Gamma_h} \tilde{\gamma}_{fa,h} \, ds, \\ \mathbf{N}\Upsilon_f \longleftrightarrow \int_{\Gamma_h} \gamma_{fa,h} \tilde{\gamma}_{fa,h} \, ds, \\ \mathbf{F}_{\gamma_{fa}} \longleftrightarrow \frac{1}{2T} \sum_{n=1}^{N_t} \int_{\Gamma_h} \left[ \frac{\partial (A_h^{(n-1)} + A_h^{(n)})}{\partial \gamma_{p,h}} + \frac{\partial \alpha_h}{\partial \gamma_{p,h}} (\mathbf{u}_h^{(n-1)} \cdot \mathbf{u}_{a,h}^{(n-1)} + \mathbf{u}_h^{(n)} \cdot \mathbf{u}_{a,h}^{(n)}) \right. \\ \quad \left. - \frac{\partial \chi_h}{\partial \gamma_{p,h}} (\mathbf{b}_{p,h}^{(n-1)} \cdot \mathbf{u}_{a,h}^{(n-1)} + \mathbf{b}_{p,h}^{(n)} \cdot \mathbf{u}_{a,h}^{(n)}) \right] \frac{\partial \gamma_{p,h}}{\partial \gamma_{f,h}} \tilde{\gamma}_{fa,h} \, ds \\ \quad + \int_{\Gamma_h} \frac{1}{T} \frac{\partial C_h}{\partial \gamma_{p,h}} \frac{\partial \gamma_{p,h}}{\partial \gamma_{f,h}} \tilde{\gamma}_{fa,h} \, ds. \end{array} \right. \quad (65)$$

## References

- [1] G. Whitesides, A. Stroock, Flexible methods for microfluidics, *Physics Today* 2001, **54**, 42-47.
- [2] H. Fallahi, J. Zhang, H. P. Phan, N. T. Nguyen, Flexible microfluidics: fundamentals, recent developments, and applications, *Micromachines* 2019, **10**, 830.
- [3] B. J. Jung, J. Kim, J. A. Kim, H. Jang, S. Seo, W. Lee, PDMS-Parylene hybrid, flexible microfluidics for real-time modulation of 3D helical inertial microfluidics, *Micromachines* 2018, **9**, 255.
- [4] G. Chen, J. Zheng, L. Liu, L. Xu, Application of microfluidics in wearable devices, *Small Methods* 2019, **3**, 1900688.
- [5] A. G. M. Michell, The limit of economy of material in frame-structures, *Phil. Mag.* 1904, **8**, 589-597.
- [6] M. Bendsoe, N. Kikuchi, Generating optimal topologies in optimal design using a homogenization method, *Comput. Methods Appl. Mech. Eng.* 1988, **71**, 197-224.
- [7] M. P. Bendsoe, O. Sigmund, *Topology optimization-theory, methods and applications*, Springer, Berlin, 2003.
- [8] O. Sigmund, On the design of compliant mechanisms using topology optimization, *Mech. Struct. Mach.* 1997, **25**, 495-526.
- [9] G. I. N. Rozvany, Aims scope methods history and unified terminology of computer-aided optimization in structural mechanics, *Struct. Multidisc. Optim.*, 2001, **21**, 90-108.
- [10] W. Akl, A. El-Sabbagh, K. Al-Mitani, A. Baz, Topology optimization of a plate coupled with acoustic cavity, *Int. J. Solids Struct.* 2008, **46**, 2060-2074.
- [11] O. Sigmund, K. G. Hougaard, Geometric properties of optimal photonic crystals, *Phys. Rev. Lett.* 2008, **100**, 153904.
- [12] T. Nomura, K. Sato, K. Taguchi, T. Kashiwa, S. Nishiwaki, Structural topology optimization for the design of broadband dielectric resonator antennas using the finite difference time domain technique, *Int. J. Numer. Methods Eng.* 2007, **71**, 1261-1296.
- [13] M. B. Duhring, J. S. Jensen, O. Sigmund, Acoustic design by topology optimization, *J. Sound Vibr.* 2008, **317**, 557-575.
- [14] A. Takezawa, M. Haraguchi, T. Okamoto, M. Kitamura, Cross-sectional optimization of whispering-gallery mode sensor with high electric field intensity in the detection domain, *IEEE. J. Sel. Top. Quant. Electron.* 2014, **20**, 1-10.
- [15] J. Andkjær, O. Sigmund, Topology optimized low-contrast all-dielectric optical cloak, *Appl. Phys. Lett.* 2011, **98**, 021112.
- [16] A. R. Diaz, O. Sigmund, A topology optimization method for design of negative permeability metamaterials, *Struct. Multidisc. Optim.* 2010, **41**, 163-177.
- [17] J. Andkjær, S. Nishiwaki, T. Nomura, O. Sigmund, Topology optimization of grating couplers for the efficient excitation of surface plasmons, *J. Opt. Soc. Am. B* 2010, **27**, 1828-1832.
- [18] E. Hassan, E. Wadbro, M. Berggren, Topology optimization of metallic antennas, *IEEE T. Antenn. Propag.* 2014, **62**, 2488-2500.
- [19] T. Borrvall, J. Petersson, Topology optimization of fluid in Stokes flow, *Int. J. Numer. Methods Fluids* 2003, **41**, 77-107.



- [20] A. Gersborg-Hansen, M.P. Bendsøe, O. Sigmund, Topology optimization of heat conduction problems using the finite volume method, *Struct. Multidisc. Optim.* 2006, **31**, 251-259.
- [21] M. Y. Wang, X. Wang, D. Guo, A level set method for structural optimization, *Comput. Methods Appl. Mech. Eng.* 2003, **192**, 227-246.
- [22] G. Allaire, F. Jouve, A. Toader, Structural optimization using sensitivity analysis and a level-set method, *J. Comput. Phys.* 2004, **194**, 363-393.
- [23] Y. M. Xie, G. P. Steven, *Evolutionary structural optimization*, Springer, 1997.
- [24] G. P. Steven, Q. Li, Y. M. Xie, Evolutionary topology and shape design for physical field problems, *Comput. Mech.* 2000, **26**, 129-139.
- [25] P. Tanskanen, The evolutionary structural optimization method: theoretical aspects, *Comput. Methods Appl. Mech. Engrg.* 2002, **191**, 47-48.
- [26] X. Huang, Y. M. Xie, A further review of ESO type methods for topology optimization, *Struct. Multidiscip. Optim.* 2010, **41**, 671-683.
- [27] K. Nabaki, J. Shen, X. Huang, Stress minimization of structures based on bidirectional evolutionary procedure, *J. Struct. Eng.* 2018, **145**, 04018256.
- [28] X. Guo, W. Zhang, W. Zhong, Doing topology optimization explicitly and geometrically — a new moving morphable components based framework, *J. Appl. Mech.* 2014, **81**, 081009.
- [29] X. Guo, W. Zhang, J. Zhang, J. Yuan, Explicit structural topology optimization based on moving morphable components (MMC) with curved skeletons, *Comput. Methods Appl. Mech. Engrg.* 2016, **310**, 711-748.
- [30] A. Takezawa, S. Nishiwaki, M. Kitamura, Shape and topology optimization based on the phase field method and sensitivity analysis, *J. Comput. Phys.* 2010, **229**, 2697-2718.
- [31] J. Guest, J. Prévost, Topology optimization of creeping fluid flows using a Darcy-Stokes finite element, *Int. J. Numer. Methods Eng.* 2006, **66**, 461-484.
- [32] S. Kreissl, G. Pingen, K. Maute, An explicit level-set approach for generalized shape optimization of fluids with the lattice Boltzmann method, *Int. J. Numer. Meth. Fluids* 2011, **65**, 496-519.
- [33] Y. Deng, Z. Liu, P. Zhang, Y. Liu, Y. Wu, Topology optimization of unsteady incompressible Navier-Stokes flows, *J. Comput. Phys.* 2011, **230**, 6688-6708.
- [34] Y. Deng, Z. Liu, J. Wu, Y. Wu, Topology optimization of steady Navier-Stokes flow with body force, *Comput. Methods Appl. Mech. Engrg.* 2013, **255**, 306-321.
- [35] Y. Deng, Z. Liu, Y. Wu, Topology optimization of steady and unsteady incompressible Navier-Stokes flows driven by body forces, *Struct. Multidisc. Optim.* 2013, **47**, 555-570.
- [36] C. B. Dilgen, S. B. Dilgen, D. R. Fuhrman, O. Sigmund, B. S. Lazarov, Topology optimization of turbulent flows, *Comput. Methods Appl. Mech. Eng.*, 2018, **331**, 363-393.
- [37] G. H. Yoon, Topology optimization for turbulent flow with Spalart-Allmaras model, *Comput. Methods Appl. Mech. Eng.*, 2016, **303**, 288-311.
- [38] Y. Deng, Z. Liu, Y. Wu, Topology optimization of capillary, two-phase flow problems, *Commun. Comput. Phys.*, 2017, **22**, 1413-1438.
- [39] M. M. Gregersen, F. Okkels, M. Z. Bazant, H. Bruus, Topology and shape optimization of induced-charge electro-osmotic micropumps, *New J. Phys.* 2009, **11**, 075019.
- [40] Y. Deng, T. Zhou, Z. Liu, Y. Wu, S. Qian, J. G. Korvink, Topology optimization of electrode patterns for electroosmotic micromixer, *Int. J. Heat Mass Tran.* 2018, **126**, 1299-1315.
- [41] G. Pingen, K. Maute, Optimal design for non-Newtonian flows using a topology optimization approach, *Comput. Math Appl.* 2010, **59**, 2340-2350.
- [42] D. H. Alonso, J. S. R. Saenz, E. C. N. Silva, Optimal design for non-Newtonian flows using a topology optimization approach, *Struct. Multidisc. Optim.* 2020, <https://doi.org/10.1007/s00158-020-02499-2>.
- [43] J. Alexandersen, C. S. Andreasen, A review of topology optimisation for fluid-based problems, *Fluids* 2020, **5**, 29.
- [44] N. Vermaak, G. Michailidis, G. Parry, R. Estevez, G. Allaire, Y. Bréchet, Material interface effects on the topology optimization of multi-phase structures using a level set method, *Struct. Multidisc. Optim.* 2014, **50**, 623-644.
- [45] O. Sigmund, S. Torquato, Design of materials with extreme thermal expansion using a three-phase topology optimization method, *J. Mech. Phys. Solids* 1997, **45**, 1037-1067.
- [46] T. Gao, W. Zhang, A mass constraint formulation for structural topology optimization with multiphase materials, *Int. J. Numer. Meth. Engng.* 2011, **88**, 774-796.

- [47] Y. J. Luo, Z. Kang, Z. F. Yue, Maximal stiffness design of two-material structures by topology optimization with nonprobabilistic reliability, *AIAA J.* 2012, 50, 1993-2003.
- [48] M. Y. Wang, X. M. Wang, "Color" level sets: a multi-phase method for structural topology optimization with multiple materials, *Comput. Methods Appl. Mech. Eng.* 2004, 193, 469-496.
- [49] S. W. Zhou, M. Y. Wang, Multimaterial structural topology optimization with a generalized Cahn-Hilliard model of multiphase transition, *Struct. Multidisc. Optim.* 2007, 33, 89-111.
- [50] P. Vogiatzis, M. Ma, S. Chen, X. Gu, Computational design and additive manufacturing of periodic conformal metasurfaces by synthesizing topology optimization with conformal mapping, *Comput. Methods Appl. Mech. Engrg.* 2018, **328**, 477-497.
- [51] L. Krog, N. Olhoff, Optimum topology and reinforcement design of disk and plate structures with multiple stiffness and eigenfrequency objectives, *Computers and Structures* 1996, 72, 535-63.
- [52] R. Ansola, J. Canales, J. A. Tárrago, J. Rasmussen, An integrated approach for shape and topology optimization of shell structures, *Computers and Structures* 2002, 80, 449-458.
- [53] B. Hassani, S. M. Tavakkoli, H. Ghasemnejad, Simultaneous shape and topology optimization of shell structures, *Struct. Multidisc. Optim.* 2013, 48, 221-233.
- [54] I. Lochner-Aldinger, A. Schumacher, Homogenization method. In: S. Adriaenssens, P. Block, D. Veenendaal, C. Williams (eds) *Shell structures for architecture-form finding and optimization*, Routledge, New York, 2014.
- [55] A. Clausen, E. Andreassen, O. Sigmund, Topology optimization of 3D shell structures with porous infill, *Acta Mechanica Sinica* 2017, 33, 778-791.
- [56] R. Dienemann, A. Schumacher, S. Fiebig, Topology optimization for finding shell structures manufactured by deep drawing, *Struct. Multidisc. Optim.* 2017, 56, 473-485.
- [57] G. H. Yoon, Topology optimization for stationary fluid-structure interaction problems using a new monolithic formulation, *Int. J. Numer. Meth. Engrg* 2010, 82, 591-616.
- [58] C. Lundgaard, J. Alexandersen, M. Zhou, C. S. Andreasen, O. Sigmund, Revisiting density-based topology optimization for fluid-structure-interaction problems, *Struct. Multidisc. Optim.* 2018, 58, 969-995.
- [59] C. S. Andreasen, A framework for topology optimization of inertial microfluidic particle manipulators, *Struct. Multidisc. Optim.* 2019, under review.
- [60] N. Aulig, I. Lepenies, *A topology optimization interface for LS-DYNA*. In: 11. LS-DYNA Forum, Ulm, 2012.
- [61] R. Behrou, M. Lawry, K. Maute, Level set topology optimization of structural problems with interface cohesion, *Int. J. Numer. Meth. Engrg.* 2017, 112, 990-1016.
- [62] M. Raulli, K. Maute, Topology optimization of electrostatically actuated microsystems, *Struct. Multidisc. Optim.* 2005, 30, 342-359.
- [63] Y. Deng, D. Mager, Y. Bai, T. Zhou, Z. Liu, L. Wen, Y. Wu, J. G. Korvink, Inversely designed micro-textures for robust Cassie-Baxter mode of super-hydrophobicity, *Comput. Methods Appl. Mech. Engrg.* 2018, 341, 113-132.
- [64] Y. Deng, Z. Liu, Y. Wang, H. Duan, J. G. Korvink, Micro-textures inversely designed with overlaid-lithography manufacturability for wetting behavior in Cassie-Baxter status, *Appl. Math. Model.* 2019, 74, 621-640.
- [65] Y. Deng, W. Zhang, Z. Liu, J. Zhu, J. G. Korvink, Fiber bundle topology optimization of hierarchical microtextures for wetting behavior in Cassie-Baxter mode, *Struct. Multidisc. Optim.* 2020, DOI: 10.1007/s00158-020-02558-8.
- [66] Y. Deng, Z. Liu, J. G. Korvink, Topology optimization on two-dimensional manifolds, *Comput. Methods Appl. Mech. Engrg.* 2020, 364, 112937.
- [67] L. Scriven, Dynamics of a fluid interface equation of motion for Newtonian surface fluids, *Chemical Engineering Science* 1960, 12, 98-108.
- [68] M. Arroyo, A. DeSimone, Relaxation dynamics of fluid membranes, *Phys. Rev. E* 2009, 79, 031915.
- [69] H. Brenner, *Interfacial transport processes and rheology*, Elsevier, 2013.
- [70] M. Rahimi, A. DeSimone, M. Arroyo, Curved fluid membranes behave laterally as effective viscoelastic media, *Soft Matter* 2013, 9, 11033-11045.
- [71] P. Rangamani, A. Agrawal, K. K. Mandadapu, G. Oster, D. J. Steigmann, Interaction between surface shape and intra-surface viscous flow on lipid membranes, *Biomechanics and Modeling in Mechanobiology* 2013, 1-13.

- [72] J. C. Slattery, L. Sagis, E. S. Oh, *Interfacial transport phenomena*, Springer Science & Business Media, 2007.
- [73] T. P. Fries, Higher-order surface FEM for incompressible Navier-Stokes flows on manifolds, *International Journal for Numerical Methods in Fluids* 2018, 88, 55-78.
- [74] S. Reuther, A. Voigt, Solving the incompressible surface Navier-Stokes equation by surface finite elements, *Physics of Fluids* 2018, 30, 012107.
- [75] L. Scriven, Dynamics of a fluid interface equation of motion for Newtonian surface fluids, *Chem. Eng. Sci.* 1960, 12, 98-108.
- [76] A. Reusken, Y. Zhang, Numerical simulation of incompressible two-phase flows with a Boussinesq-Scriven surface stress tensor, *Int. J. Numer. Meth. Fl.* 2013, 73, 1042-1058.
- [77] B. Lazarov, O. Sigmund, Filters in topology optimization based on Helmholtz type differential equations, *Int. J. Numer. Methods Eng.* 2011, 86, 765-781.
- [78] F. Wang, B. S. Lazarov, O. Sigmund, On projection methods, convergence and robust formulations in topology optimization, *Struct. Multidiscip. Optim.* 2011, 43, 767-784.
- [79] J. Guest, J. Prévost, T. Belytschko, Achieving minimum length scale in topology optimization using nodal design variables and projection functions, *Int. J. Numer. Methods Eng.* 2004, 61, 238-254.
- [80] M. Hinze, R. Pinnau, M. Ulbrich, S. Ulbrich, *Optimization with PDE constraints*, Springer, Berlin, 2009.
- [81] G. Dziuk, C. M. Elliott, Finite element methods for surface PDEs, *Acta Numerica*, 2013, 22, 289-396.
- [82] K. Svanberg, The method of moving asymptotes: a new method for structural optimization, *Int. J. Numer. Meth. Engng.* 1987, 24, 359-373.
- [83] H. C. Elman, D. J. Silvester, A. J. Wathen, *Finite elements and fast iterative solvers: with applications in incompressible fluid dynamics*, Oxford University Press, 2006.
- [84] U. M. Ascher, L. R. Petzold, *Computer methods for ordinary differential equations and differential-algebraic equations*, SIAM, Philadelphia, 1998, ISBN 0-89871-412-5.
- [85] E. Süli, D. Mayers, *An introduction to numerical analysis*, Cambridge University Press, 2003, ISBN 0-521-00794-1.
- [86] <https://www.pardiso-project.org/>.